Article
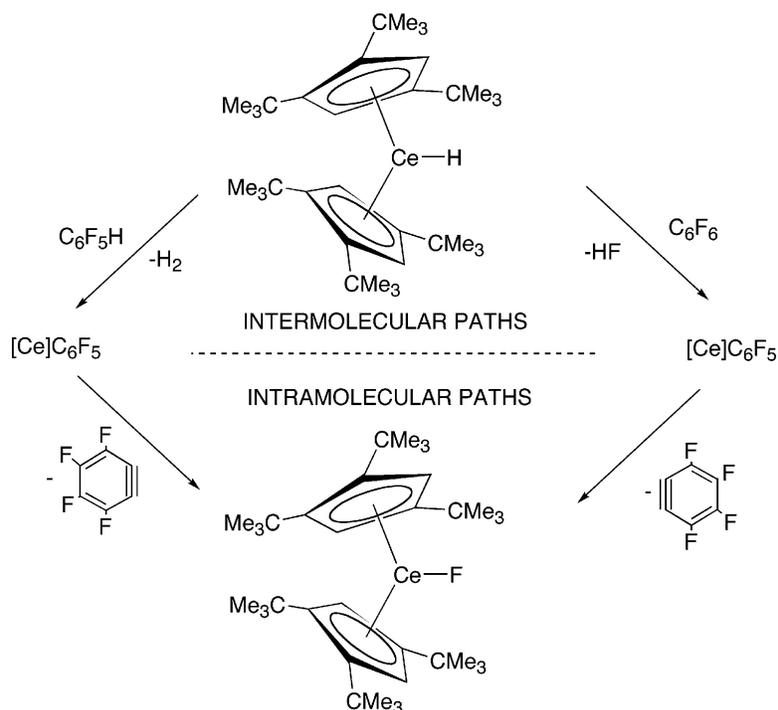
Hydrogen for Fluorine Exchange in CF and CFH by Monomeric [1,3,4-(MeC)CH]CeH: Experimental and Computational Studies

Laurent Maron, Evan L. Werkema, Lionel Perrin, Odile Eisenstein, and Richard A. Andersen

More About This Article

Additional resources and features associated with this article are available within the HTML version:

- Supporting Information
- Links to the 26 articles that cite this article, as of the time of this article download
- Access to high resolution figures
- Links to articles and content related to this article
- Copyright permission to reproduce figures and/or text from this article

Hydrogen for Fluorine Exchange in C_6F_6 and C_6F_5H by Monomeric $[1,3,4-(Me_3C)_3C_5H_2]_2CeH$: Experimental and Computational Studies

Laurent Maron,*,[†] Evan L. Werkema,[‡] Lionel Perrin,[§] Odile Eisenstein,*,[§] and Richard A. Andersen*,[‡]

Contribution from the Laboratoire de Physique Quantique, UMR 5626, IRSAMC, Université Paul Sabatier, 118 Route de Narbonne, 31064 Toulouse Cedex 4, France, Chemistry Department and Chemical Sciences Division of Lawrence Berkeley National Laboratory, University of California, Berkeley, California 94720, and LSDSMS, UMR 5636 Université Montpellier 2, 34095 Montpellier Cedex 5, France

Received August 13, 2004; E-mail: laurent.maron@irsamc.ups-tlse.fr; odile.eisenstein@univ-montp2.fr; raandersen@lbl.gov

Abstract: The net reaction of monomeric Cp'_2CeH [$Cp' = 1,3,4-(Me_3C)_3(C_5H_2)$] in C_6D_6 with C_6F_6 is Cp'_2-CeF, H_2, and tetrafluorobenzyne. The pentafluorophenylmetallocene, $Cp'_2Ce(C_6F_5)$, is formed as an intermediate that decomposes slowly to Cp'_2CeF and C_6F_4 (tetrafluorobenzyne), and the latter is trapped by the solvent C_6D_6 as a [2+4] cycloadduct. In C_6F_5H, the final products are also Cp'_2CeF and H_2, which are formed from the intermediates $Cp'_2Ce(C_6F_5)$ and $Cp'_2Ce(2,3,5,6-C_6F_4H)$ and from an unidentified metallocene of cerium and the [2+4] cycloadducts of tetra- and trifluorobenzyne with C_6D_6. The hydride, fluoride, and pentafluorophenylmetallocenes are isolated and characterized by X-ray crystallography. DFT-(B3PW91) calculations have been used to explore the pathways leading to the observed products of the exergonic reactions. A key step is a H/F exchange reaction which transforms C_6F_6 and the cerium hydride into C_6F_5H and Cp'_2CeF. This reaction starts by an η^1-F$-C_6F_5$ interaction, which serves as a hook. The reaction proceeds via a σ bond metathesis where the fluorine ortho to the hook migrates toward H with a relatively low activation energy. All products observed experimentally are accommodated by pathways that involve C$-$F and C$-$H bond cleavages.

Introduction

The hydrogen for fluorine exchange in fluorocarbons is a thermodynamically favorable reaction that does not occur in absence of a catalyst.[1] For example, passing a mixture of C_6F_6 and dihydrogen over Pd/C or Pt/C at 300 °C gives a mixture of aromatic hydrofluorocarbons; Pt/C at 58% conversion gives C_6F_5H and mixed isomers of $C_6F_4H_2$ and $C_6F_3H_3$ in a 4:3:1 ratio.[2] The exchange reaction is exothermic when the sum of the C$-$F and H$-$H bond enthalpies is less than those of C$-$H and H$-$F in eq 1, where the bond dissociation enthalpies are in parentheses in units of kcal mol^{-1}.

$$C_6F_5-F \ + \ H-H \ \rightarrow \ C_6F_5H \ + \ HF$$
$$(154)^3 \qquad (105)^4 \qquad (x) \qquad (135)^{4,5} \qquad (1)$$
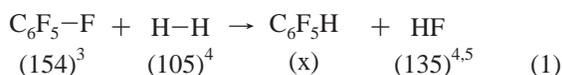
Although the bond disruption enthalpy of C_6F_5-H is unknown, the reaction will be exothermic if the C$-$H bond enthalpy is greater than 125 kcal mol^{-1}, which is reasonable since the bond dissociation energy (BDE) of C_6H_4F-H is 126 kcal mol^{-1}.[3] Thus, the exothermicity of a H/F exchange reaction is driven

by the large H$-$F bond disruption enthalpy, which in general implies that when H_2 is replaced by M$-$H, the reaction will be exothermic when the M$-$F bond enthalpy is larger than the M$-$H bond enthalpy by about 30 kcal mol^{-1}. This condition is met by the f-block and early d-transition metals. Lanthanide fluoride bonds are strong; the averaged Ce$-$F bond enthalpy of $CeF_3(g)$ is 153 kcal mol^{-1},[6] which implies that the H/F exchange will be exothermic, provided that the lanthanide$-$hydride bond enthalpy is less than about 125 kcal mol^{-1}. Although the averaged bond enthalpy of M$-$H in $MH_3(g)$ is unknown, it is unlikely to be greater than 100 kcal mol^{-1} since the M$-$H BDE in $Cp*_2LaH$ and $Cp*_2LuH$ is 67 kcal mol^{-1}.[7] The rate, of course, is unknown.

Lanthanide metals in gas phase will defluorinate fluorocarbons.[8] For example, $Ce^+(g)$ defluorinates C_6F_6 giving CeF^+-(g), the radical $C_6F_5^{\bullet}$, $CeF_2^+(g)$, and C_6F_4 (a benzyne).[9] In

---

† Université Paul Sabatier.
‡ University of California.
§ Université Montpellier 2.

(1) Hudlicky, M. *J. Fluorine Chem.* **1989**, *44*, 345.
(2) Florin, R. E.; Pummer, W. J.; Wall, L. A. *J. Res. Natl. Bur. Stand.* **1959**, *62*, 119.

(3) Smart, B. E. In *Chemistry of Functional Groups*; Patai, S., Rappoport, Z., Eds.; Wiley: New York, 1983; Suppl. D, Chapter 14.
(4) Dasent, W. E. *Inorganic Energetics*, 2nd ed.; Cambridge University Press: Cambridge, U.K., 1982; p 103.
(5) Slayden, S. W.; Liebman, J. F.; Mallard, W. G. In *Chemistry of Functional Groups. The chemistry of halides, pseudohalides and azides*; Patai, S., Rappoport, Z., Eds.; Wiley: Chichester, U.K., 1995; Suppl D2, p 387.
(6) Pankratz, L. B. *Thermodynamic Properties of Halides, Bulletin 674, Bureau of Mines*, 1984.
(7) Nolan, S. P.; Stern, D.; Hedden, D.; Marks, T. J. *Bonding Energetics in Organometallic Chemistry*; ACS Symposium Series 428; American Chemical Society: Washington, DC, 1990; pp 159−174.
(8) Mazurek, U.; Schwarz, H. *Chem. Commun.* **2003**, 1321.

addition, the metallocene $(Me_5C_5)_2Yb$ abstracts a fluorine atom from C_6F_6 giving $[(Me_5C_5)_2Yb]_2(\mu\text{-F})$,[10] and $(MeC_5H_4)_3UCMe_3$ exchanges the CMe_3 with F in C_6F_6.[11] The general subject of intermolecular C—F activation has been extensively studied and several reviews are available, largely within the framework of oxidative addition reactions.[8,12] Computational studies have shown that the C—F activation may be exothermic but that a high activation barrier is usually observed with late transition-metal systems.[13] In early transition metals, the activation barrier is generally lower and several cases of H/F exchange have been observed.[14] The reactions of bare metal centers have been analyzed by computational methods, showing that electron transfer as well as oxidative insertion paths are possible.[15]

In this paper, we show that a monomeric metallocene hydride of cerium undergoes H/F exchange with fluoroaromatics and DFT calculations provide details about the relative activation barriers for the reaction pathways.

Results

General Strategy. The DFT calculations of the possible reaction pathways for H/F exchange are carried out on a monomeric $(C_5H_5)_2MH$ (Cp_2MH) reactant and a $(C_5H_5)_2MF$ (Cp_2MF) product in the gas phase. It is essential that the synthetic studies begin and end with a monomeric metallocene hydride and fluoride derivative, respectively, in order that the experimental and calculational results track each other as closely as possible. Since no monomeric metallocene lanthanide hydrides or fluorides are known, synthetic studies were initiated with the goal of making them. In general, the base-free metallocene hydrides are dimeric in the solid state and in solution.[16] The dimeric cerium hydrides, $(C_5Me_5)_4Ce_2(\mu\text{-H})_2$ and $[1,3\text{-}(Me_3C)_2C_5H_3]_4Ce_2((\mu\text{-H})_2$, are known.[17,18] A tiny number of metallocene lanthanide fluorides are known[10,19,20] and only
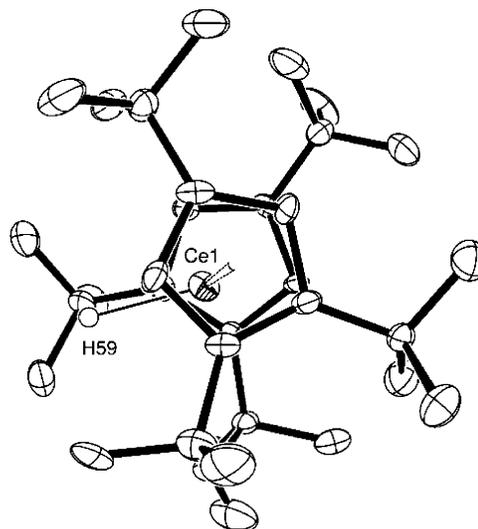
Figure 1. ORTEP diagram of Cp'_2CeH (50% probability ellipsoids). The hydrogen atoms on the Cp' ligands were placed in calculated positions; $H(59)$, the hydride ligand, was found in the difference Fourier map and refined with isotropic thermal parameters. Ce—C (ave) = 2.81(2) Å, Ce—Cp(ring centroid) (ave) = 2.53 Å, Ce—H = 1.90(5) Å, Cp(ring centroid)—Ce—Cp(ring centroid) = 155°, Cp(ring centroid)—Ce—H (ave) = 101°.

one, $[1,3\text{-}(SiMe_3)_2C_5H_3]_4Sm_2(\mu\text{-F})_2$, contains symmetrical bridging fluorides.[21] Our focus is on the metallocene derivatives of cerium since the $4f^1$ electron configuration simplifies the interpretation of their magnetic properties. In addition, one of our long-term interests is comparison of the chemical and physical properties between the 4f and 5f block metals with identical radii, that is, Ce(III) and U(III). The 1,3-di-*tert*-butylcyclopentadienyl ligand yields the dimeric cerium hydride, $[1,3\text{-}(Me_3C)_2C_5H_3]_4Ce_2(\mu\text{-H})]_2$,[18] suggesting that increasing the number of Me_3C-groups on the cyclopentadienyl ring will yield a monomeric hydride, a deduction that is correct.

Synthetic Studies. The synthetic sequence begins with the synthesis of the bis (1,3,4-tri-*tert*-butylcyclopentadienyl) cerium triflate, Cp'_2CeOTf, then replacing the triflate by a benzyl group; the synthesis details are in the Experimental Section. Addition of dihydrogen to the benzyl derivative in pentane gives the deep purple hydride, Cp'_2CeH, mp 152–155 °C, which may be crystallized from pentane. The hydride gives a $(M-2)^+$ molecular ion in the mass spectrum, but the Ce—H stretching frequency could not be identified in the infrared spectrum, even when directly compared with the deuteride (prepared by using D_2 rather than H_2), nor could the Ce—H resonance be observed in the ^1H NMR spectrum. The ^1H NMR spectrum clearly shows the paramagnetic isotropic shifts for the two types of Me_3C-groups in a 2:1 area ratio and the equivalent ring methyne resonances; the details are given in the Experimental Section. Figure 1 shows an ORTEP diagram of the hydride; important structural parameters are given in the figure caption. The solid-state structure clearly shows that the hydride is a monomer.

The fluoride is prepared by allowing Cp'_2CeCH_2Ph to react with $BF_3\cdot OEt_2$ in pentane, a method used previously.[22] The fluoride, mp 164–167 °C, crystallizes from pentane as orange crystals that yield a monomeric molecular ion in the gas-phase

(9) Cornehl, H. H.; Hornung, G.; Schwarz, H. *J. Am. Chem. Soc.* **1996**, *118*, 9960.
(10) Burns, C. J.; Andersen, R. A. *J. Chem. Soc., Chem. Commun.* **1989**, 136.
(11) Weydert, M.; Andersen, R. A.; Bergman, R. G. *J. Am. Chem. Soc.* **1993**, *115*, 8837.
(12) Kiplinger, J. L.; Richmond, T. G.; Osterberg, C. E. *Chem. Rev.* **1994**, *94*, 373. Richmond, T. G. *Top. Organomet. Chem.* **1999**, *3*, 243. Burdeniuc, J.; Jedlicka, B.; Crabtree, R. H. *Chem. Ber./Recueil* **1997**, *130*, 145. Murphy, E. F.; Murugavel, R.; Roesky, H. W. *Chem. Rev.* **1997**, *97*, 3425. Alonso, F.; Beletskaya, I. P.; Yus, M. *Chem. Rev.* **2002**, *102*, 4009. Braun, T.; Perutz, R. N. *Chem. Commun.* **2002**, 2749. Jones, W. D. *Dalton Trans.* **2003**, 3991.
(13) Su, M. D.; Chu, S.-Y. *J. Am. Chem. Soc.* **1997**, *119*, 10178. Bosque, R.; Fantacci, S.; Clot, E.; Maseras, F.; Eisenstein, O.; Perutz, R. N.; Renkema, K. B.; Caulton, K. G. *J. Am. Chem. Soc.* **1998**, *120*, 12634. Gérard, H.; Davidson, E. R.; Eisenstein, O. *Mol. Phys.* **2002**, *100*, 533. Reinhold, M.; McGrady, J. E.; Perutz, R. N. *J. Am. Chem. Soc.* **2004**, *126*, 5268.
(14) Edelbach, B. L.; Rahman, A. K. F.; Lachicotte, R.; Jones, W. D. *Organometallics* **1999**, *18*, 3170. Edelbach, B.; Kraft, B. M.; Jones, W. D. *J. Am. Chem. Soc.* **1999**, *121*, 10327. Kraft, B. M.; Lachicotte, R. J.; Jones, W. D. *J. Am. Chem. Soc.* **2000**, *122*, 8559. Kraft, B. M.; Jones, W. D. *J. Organomet. Chem.* **2002**, *658*, 132. Watson, L. A.; Yandulov, D. V.; Caulton, K. G. *J. Am. Chem. Soc.* **2001**, *123*, 603. Yang, H.; Gao, H.; Angelici, R. J. *Organometallics* **1999**, *18*, 2285. Turculet, L.; Tilley, T. D. *Organometallics* **2002**, *21*, 3961. Clot, E.; Mégret, C.; Kraft, B. M.; Eisenstein, O.; Jones, W. D. *J. Am. Chem. Soc.* **2004**, *126*, 5647.
(15) Harvey, J. N.; Schröder, D.; Koch, W.; Danovich, D.; Shaik, S.; Schwarz, H. *Chem. Phys. Lett.* **1997**, *278*, 391. Chen, Q.; Freiser, B. S. *J. Phys. Chem. A* **1998**, *102*, 3343. Zhang, D.; Liu, C.; Bi, S. *J. Phys. Chem. A* **2002**, *106*, 4153.
(16) Ephritikhine, M. *Chem. Rev.* **1997**, *97*, 2193. Schaverien, C. J. *Adv. Organomet. Chem.* **1994**, *36*, 283. Jeske, G.; Lauke, H.; Mauermann, H.; Swepston, P. N.; Schumann, H.; Marks, T. J. *J. Am. Chem. Soc.* **1985**, *107*, 8091.
(17) Heeres, H. J.; Renkema, J.; Booij, M.; Meetsma, A.; Teuben, J. H. *Organometallics* **1988**, *7*, 2495.
(18) Gunko, Y. K.; Bulychev, B. M.; Soloveichik, G. L.; Belsky, V. K. *J. Organomet. Chem.* **1992**, *424*, 289.
(19) Burns, C. J.; Berg, D. J.; Andersen, R. A. *J. Chem. Soc., Chem. Commun.* **1987**, 272.
(20) Watson, P. L.; Tulip, T. H.; Williams, I. *Organometallics* **1990**, *9*, 1999.
(21) Xie, Z. W.; Liu, Z. X.; Xue, F.; Mak, T. C. W. *J. Organomet. Chem.* **1997**, *539*, 127.
(22) Lukens, W. W.; Beshouri, S. M.; Blosch, L. L.; Stuart, A. L.; Andersen, R. A. *Organometallics* **1999**, *18*, 1235.

Scheme 1
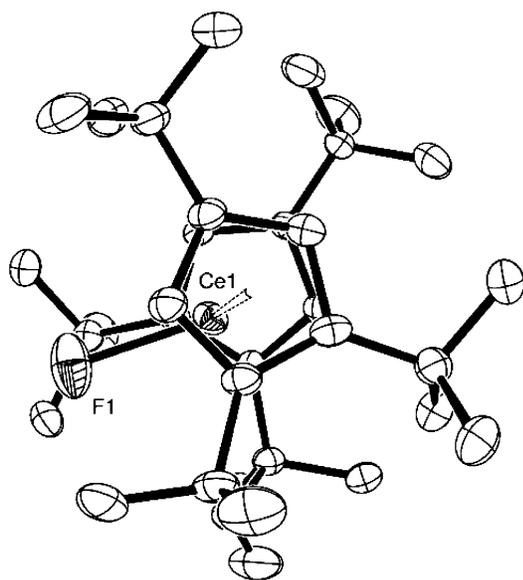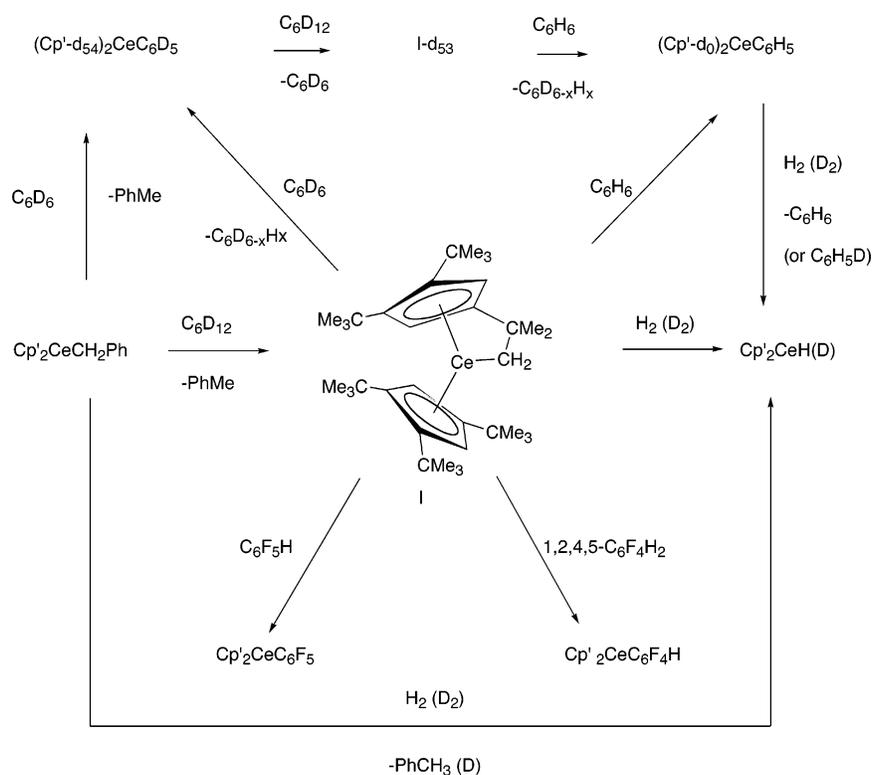
Figure 2. ORTEP diagram of Cp′₂CeF (50% probability ellipsoids). All the non-hydrogen atoms were refined anisotropically and the hydrogen atoms were placed in calculated positions. Ce−C (ave) = 2.82(2) Å, Ce−Cp-(ring centroid) (ave) = 2.55 Å, Ce−F = 2.165(2) Å, Cp(ring centroid)−Ce−Cp(ring centroid) = 149°, Cp(ring centroid)−Ce−F (ave) = 105(2)°.

mass spectrum. The ^{1}H NMR spectrum at 20 °C shows resonances for the two inequivalent types of Me₃C groups in a 2:1 ratio and a single-ring methyne resonance. The fluoride sublimes at 140 °C in a vacuum and crystals suitable for an X-ray study were grown in this way. An ORTEP diagram of the monomeric fluoride is shown in Figure 2 and some bond parameters are given in the figure caption.

The hydride and fluoride derivatives are stable in C₆D₆ and C₆D₁₂ solution for an indefinite period of time. In contrast, the

benzyl derivative though stable at 25 °C in the solid state, gives a (M-PhCH₃)⁺ molecular ion in the mass spectrum. In C₆D₆ solution, the CMe₃ resonances slowly disappear from the ^{1}H NMR spectrum as the intensity of the C₆H₆₋ₓDₓ resonances increase relative to an internal standard as the resonances due to PhMe appear. Over the course of a week at 65 °C, all the CMe₃ resonances disappear. Replacing essentially all of the C₆D₆ by C₆H₆ regenerates Me₃C resonances with chemical shifts different from those of the benzyl derivative. The new resonances have intensities and a coupling pattern (the meta and para resonances appear as doublet and triplet, respectively) consistent with those expected for Cp′₂CePh. Thus, the CMe₃ groups undergo reversible H/D exchange with C₆D₆ or C₆H₆, with formation of a Cp′₂CeC₆H₅ or Cp′₂CeC₆D₅ species. In C₆D₁₂ solvent, the resonances due to toluene appear after 3 h at 65 °C in addition to another set of rather broadened resonances that appears as five equal area resonances and two additional resonances of about one-third their intensity. These observations suggest that this species is the chiral metallacycle [(Me₃C)₃C₅H₂)][Me₃C)₂C₅H₂(CMe₂CH₂)]Ce, a deduction consistent with the reactions shown in Scheme 1; experimental details are in the Experimental Section. A related metallacyle has been observed by heating (Me₅C₅)₂CeCH(SiMe₃)₂ in C₆D₁₂, which is a tetramer in the solid state.[23]

On a synthetic scale (ca. 1 g), warming Cp′CeCH₂Ph in pentane for 12 h gives a deep purple solution, which yields a purple glassy solid that cannot be persuaded to crystallize. The ^{1}H NMR spectrum in C₆D₁₂ is identical to that observed in the NMR tube experiment mentioned above. Refluxing a solution of Cp′₂CeCH₂Ph in C₆H₆ for 3 days gives a red solution, which yields a red powder whose elemental analysis indicates that the stoichiometry is Cp′₂CeC₆H₅. The ^{1}H NMR spectrum in C₆D₆

(23) Booij, M.; Meetsma, A.; Teuben, J. H. *Organometallics* **1991**, *10*, 3246.
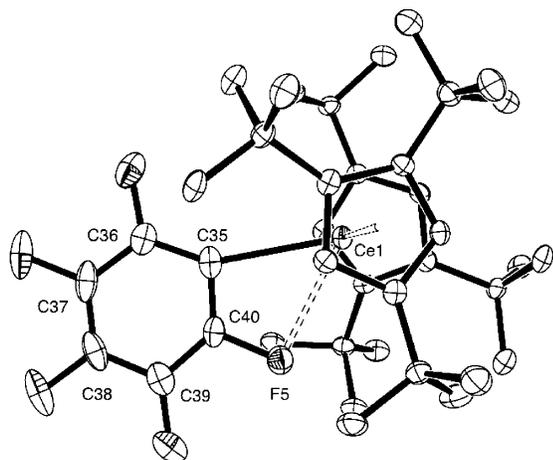
Figure 3. ORTEP diagram of Cp$'_2$Ce(C$_6$F$_5$) (50% probability ellipsoids). All the non-hydrogen atoms were refined anisotropically and the hydrogen atoms were placed in calculated positions. Ce−C (ave) = 2.81(5) Å, Ce−Cp(ring centroid) (ave) = 2.54 Å, Ce−C(35) = 2.621(4) Å, Ce···F(5) = 2.682(2), Cp(ring centroid)−Ce−Cp(ring centroid) = 147°, Cp(ring centroid)−Ce−C(35) = 107(1)°, Cp(ring centroid)−Ce−F(5) (ave) = 101(1)°, Ce−C(35)−C(36) = 149.7(3)°, Ce−C(35)−C(40) = 97.5(3)°.

is identical to that observed in the NMR tube experiment described above. Although neither metallacycle nor phenyl derivative is obtained in crystalline form, the sequence of reactions in Scheme 1 is consistent with the formulation given.

Further proof that the metallacycle formulation is correct is derived by dissolving it in a mixture of C$_6$F$_5$H and C$_6$D$_{12}$ and observing a new set of Me$_3$C-resonances in a 1:2 ratio. On a synthetic scale, dissolving the metallacycle in an excess of C$_6$F$_5$H in pentane yields an orange solution from which orange crystals may be isolated, whose ^{1}H NMR spectrum is identical to that observed in the mixing experiment. The crystals decompose rather violently on attempted melting in a sealed melting point capillary at about 125 °C; extracting the residue into C$_6$D$_6$ and examining the ^{1}H NMR spectrum shows resonances due to Cp$'_2$CeF, as well as several unidentified resonances. The thermal behavior is presumably the reason for the incomprehensible mass spectrum. Fortunately, single crystals of Cp$'_2$CeC$_6$F$_5$ suitable for X-ray studies are obtained from pentane and an ORTEP diagram is shown in Figure 3. As can been seen, the carbon atom of the C$_6$F$_5$ group C(35) is located close to the idealized C_2 axis but the Ce−C(35)−C(36,40) angles are very anisotropic because of a short Ce···F−C(ortho) contact of 2.682(2) Å. A pair of close ortho-F···Sm contacts of 2.531(8) Å and 2.539(7) Å were found in dimeric (C$_5$Me$_5$)$_4$-Sm$_2$(C$_6$F$_5$)$_2$ and in monomeric (C$_5$Me$_5$)Yb(C$_6$F$_5$)(thf)$_3$ where the ortho-F···Yb distance is 3.162 Å.[24] In solution at 25 °C, the ^{1}H and ^{19}F NMR spectra are not consistent with the solid-state crystal structure, where the idealized symmetry is C_1 and all of the CMe$_3$ groups and F atoms are inequivalent. The ^{1}H NMR absorptions change as a function of temperature and the CMe$_3$ resonance of area 2 decoalesces into two equal area resonances while the other CMe$_3$ resonance of area 1 has a normal temperature dependence (Figure 4), giving a $\Delta G^{\#}_{TC}$ = 10 kcal mol^{-1}. The 25 °C ^{19}F NMR spectrum consists of three resonances, two of area 2 and one of area 1. One of the area 2 resonances is broad ($\nu_{1/2}$ = 480 Hz), probably because of the
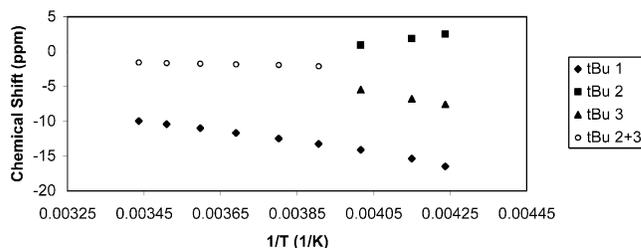
Figure 4. Plot of chemical shift (δ) vs $1/T$ for Cp$'_2$CeC$_6$F$_5$ in PhMe-d_8.

ortho-F, and the other two resonances are a doublet and triplet at δ −161 and δ −158 in area ratio 2:1, respectively, J = 18 Hz. Cooling shifts the resonances and the coupling between meta-F, and para-F disappears as the resonances broaden but do not decoalesce to −50 °C. The 2:1 pattern of the CMe$_3$ resonances changing to a 1:1:1 pattern at low temperature is consistent with a metallocene whose idealized symmetry changes from C_{2v} to C_s, where the mirror plane is coplanar with the C$_6$F$_5$ ring. Several physical processes can account for loss of the time-averaged C_2-axis and mirror plane, two of which are slowing the librational motion of the Cp$'$-rings about their pseudo-C_5 axis and slowing the rocking motion of the C$_6$F$_5$ ring in the mirror plane. If the C$_6$F$_5$ ring rocking is slowed by a Ce···F interaction, as observed in the crystal structure, and if the Cp$'$ rings undergo libration, then the CMe$_3$ groups will appear as a 1:1:1 pattern and the F nuclei in the C$_6$F$_5$ ring may appear as distinct resonances or as broadened features depending upon how much the chemical shift changes as a function of temperature. In this context, the librational motion of the Cp$'$ rings in Cp$'_2$CeH and Cp$'_2$CeF is not slowed, that is, the 2:1 pattern is observed at −90 °C. Further studies are needed to define the physical process responsible for the fluxional processes.

Solution NMR Mixing Experiments, H/F Exchange Reactions. C$_6$F$_6$. When an excess of C$_6$F$_6$ is added to Cp$'_2$CeH in C$_6$D$_6$ in an NMR tube, the purple color of the hydride instantaneously turns orange and a gas is evolved. Examination of the ^{1}H NMR spectrum shows that the resonances due to Cp$'_2$-CeH are absent and new sets of resonances due to Cp$'_2$CeF, Cp$'_2$CeC$_6$F$_5$, and dihydrogen appear. Over time, the resonances due to Cp$'_2$CeF increase in intensity at the expense of those due to Cp$'_2$CeC$_6$F$_5$. These events are symbolized by the unbalanced eqs 2 and 3.

$$Cp'_2CeH + C_6F_6 \rightarrow Cp'_2CeF + Cp'_2CeC_6F_5 + H_2 \quad (2)$$

$$Cp'_2CeC_6F_5 \rightarrow Cp'_2CeF + C_6F_4 \quad (3)$$

Examination of the ^{19}F NMR spectrum of this mixture shows resonances due to Cp$'_2$CeC$_6$F$_5$ and an AA′BB′ pattern whose chemical shifts and coupling pattern are identical to the Diels−Alder adduct **1**, X = D, between tetrafluorobenzyne and benzene-d_6.[25] Hydrolysis of the mixture with H$_2$O and injection into a GCMS gives the M$^+$ for **1**, X = D. Repeating the experiment, but replacing the C$_6$D$_6$ with C$_6$H$_6$ followed by hydrolysis with H$_2$O and injection into a GCMS gives M$^+$ for **1**, X = H, Y = F. Thus, Cp$'_2$CeC$_6$F$_5$ decomposes by forming Cp$'_2$CeF and tetrafluorobenzyne that is trapped by the solvent
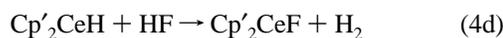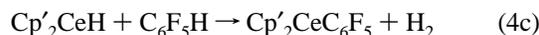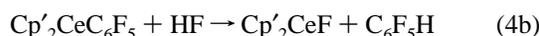
(24) Castillo, I.; Tilley, T. D. *J. Am. Chem. Soc.* **2001**, *123*, 10526. Deacon G. B.; Forsyth, C. M. *Organometallics* **2003**, *22*, 1349.

(25) Fruchier, A.; Claramunt, R. M.; Elguero, J.; Carmona, D.; Esteban, M. *Bull Soc. Chim. Belg.* **1992**, *101*, 697. Brewer, J. P. N.; Eckhard, I. F.; Heaney, H.; Marples, B. A. *J. Chem. Soc. C* **1968**, 664.

benzene, a common decomposition pattern of pentafluorophen-ylmetal compounds.[26]
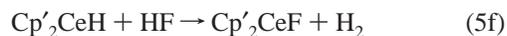

X = H or D
Y = H or F
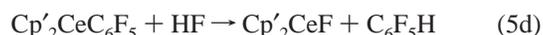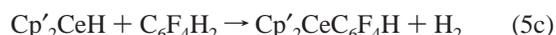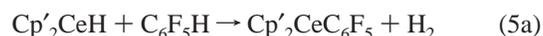
1

X = F, H or D

2
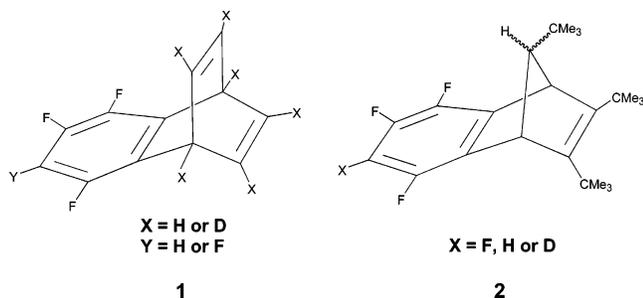
The origin of dihydrogen is less readily explained, though the net reactions symbolized in eq 4a–d may be suggested. Equation 4a is an intermolecular C–F activation, 4c is a C–H activation, and both yield $Cp'_2CeC_6F_5$, which ultimately yields Cp'_2CeF. Equation 4b and 4d destroys the HF that is formed producing Cp'_2CeF. No intermediates are detected, other than $Cp'_2CeC_6F_5$, and only the reaction in 4c can be easily tested, since we do not have facilities to deal with anhydrous HF.

$$Cp'_2CeH + C_6F_6 \rightarrow Cp'_2CeC_6F_5 + HF \qquad (4a)$$

$$Cp'_2CeC_6F_5 + HF \rightarrow Cp'_2CeF + C_6F_5H \qquad (4b)$$

$$Cp'_2CeH + C_6F_5H \rightarrow Cp'_2CeC_6F_5 + H_2 \qquad (4c)$$

$$Cp'_2CeH + HF \rightarrow Cp'_2CeF + H_2 \qquad (4d)$$

Neither dihydroanthracene nor addition of H_2 or D_2 alters the reaction, and no anthracene or hydrogenated products are detected. However, changing the solvent from C_6D_6 to C_6D_{12} removes the trap for tetrafluorobenzyne, and the Cp'-ring is now the trap. In C_6D_{12}, $Cp'_2CeC_6F_5$ decomposes to Cp'_2CeF and a new organic product over 12 h at 60 °C. Hydrolysis with D_2O or H_2O and injection into the GCMS shows one major fluorinated organic compound with $M^+ = 382$ along with Cp'D or Cp'H. This organic product is likely to be **2**, X = F, the [2+4] cycloaddition product of C_6F_4, and the substituted cyclopentadienyl ring. The ^{19}F NMR spectrum consists of an AA'BB' pattern similar to that found in **1**, and the ^{1}H NMR spectrum shows two CMe₃ resonances in a 2:1 ratio. Other isomers of **2** could be formed, since low intensity absorptions are visible in the ^{1}H and ^{19}F NMR spectra, but **2** is the major isomer formed. When deutero metallocene, $\{[C(CD_3)_3]_3C_5H_2\}_2$-$CeC_6F_5$, is allowed to decompose in C_6D_{12} and the residue hydrolyzed with H_2O and analyzed by GCMS, the M^+ at 410 is observed, implying that the source of the "other" hydrogen is a ring –CMe₃. Close inspection of the ^{19}F NMR spectrum resulting from decomposition of $Cp'_2CeC_6F_5$ in C_6D_6 shows that the **2**, X = F is also present to the extent of about 10%, suggesting that the Cp'-ring can compete with C_6D_6 as a trap for tetrafluorobenzyne. Cyclopentadiene and its anion are capable of trapping benzyne[27] and furan and other dienes trap tetrafluorobenzyne[28] so the suggestion that Cp' traps tetrafluo-robenzyne is not without precedent.

(26) Banks, R. E. *Fluorocarbons and their Derivatives*, 2nd ed.; MacDonald & Co: London, 1970; Chapter 5. Cohen, S. C.; Massey, A. G. *Adv. Fluorine Chem.* **1970**, *6*, 83.
(27) Hoffmann, R. W. *Dehydrobenzene and cycloalkynes*; Academic Press: New York, 1967. Buske, G. R.; Ford, W. T. *J. Org. Chem.* **1976**, *41*, 1995.
(28) Wenk, H. H.; Sander, W. *Chem. Eur. J.* **2001**, *7*, 1837.

C₆F₅H. Adding an excess of C_6F_5H to Cp'_2CeH dissolved in C_6D_6 in an NMR tube changes the purple solution to an orange one with liberation of a gas. The ^{1}H NMR spectrum shows resonances due to Cp'_2CeF and $Cp'_2CeC_6F_5$, and two new sets of paramagnetic resonances in a ratio of 6:2:4:1, assuming the resonances are all due to CMe₃ groups and H_2. Integration of the initial and final CMe₃ resonances relative to an internal standard shows that the conversion is quantitative. Over time, all of the resonances disappear, except those due to Cp'_2CeF, which is the only cerium containing metallocene at the end of the reaction. The second most abundant set of resonances is identical to those formed by addition of the metallacycle to 1,2,4,5-tetrafluorobenzene (Scheme 1) in C_6D_{12} implying that its identity is $Cp'_2Ce(2,3,5,6\text{-}C_6F_4H)$. When the latter solution is evaporated to dryness, dissolved in C_6D_{12}, and heated to 65 °C for 12 h, resonances due to Cp'_2CeF form. The liberated C_6F_3H is trapped by the Cp' ring, since the ^{19}F NMR spectrum shows a new ABCX (**2**, X = H) pattern as well as resonances in the ^{1}H NMR spectrum due to **2**, X = H. Hydrolysis with H_2O and injection into a GCMS gives a M^+ due to **2**, X = H. When the trifluorobenzyne is trapped with C_6D_6, the NMR spectra and GCMS are consistent with **1**, X = D, Y = H.[29] The remaining set of new resonances in the original reaction of Cp'_2CeH and C_6F_5H is due to an unknown cerium-containing product. This set of resonances forms exclusively when a solution of the metallacycle is added to $Cp'_2Ce(2,3,5,6\text{-}C_6F_4H)$ in C_6D_{12}, suggesting that the unknown compound is Cp'_2Ce-$(1,4\text{-}C_6F_4)CeCp'_2$. Hydrolysis with H_2O gives 1,2,4,5-tetrafluo-robenzene as the only substance detected by ^{19}F NMR spectroscopy consistent with this deduction. The net reactions that account for the products conclusively identified in the NMR experiments may be written in eq 5a–f.

$$Cp'_2CeH + C_6F_5H \rightarrow Cp'_2CeC_6F_5 + H_2 \qquad (5a)$$

$$Cp'_2CeH + C_6F_5H \rightarrow Cp'_2CeC_6F_4H + HF \qquad (5b)$$

$$Cp'_2CeH + C_6F_4H_2 \rightarrow Cp'_2CeC_6F_4H + H_2 \qquad (5c)$$

$$Cp'_2CeC_6F_5 + HF \rightarrow Cp'_2CeF + C_6F_5H \qquad (5d)$$

$$Cp'_2CeC_6F_4H + HF \rightarrow Cp'_2CeF + C_6F_4H_2 \qquad (5e)$$

$$Cp'_2CeH + HF \rightarrow Cp'_2CeF + H_2 \qquad (5f)$$

The reaction symbolized in 5a and 5b are intermolecular C–H and C–F activations, respectively, while those in the remaining equations result from secondary reactions. Since the reactions between Cp'_2CeH and $C_6F_{6-x}H_x$ ($x = 0$, 1) are rapid and the only intermediate that is detected is either $Cp'_2CeC_6F_5$ or Cp'_2-CeC_6F_4H, only the net reaction symbolized by eqs 4 and 5 can be written with confidence. The mechanism of the H/F chemical exchange in Cp'_2CeH is unknown from the experiments described. In the next section, DFT calculations provide guidance about the relative thermodynamic quantities and kinetic barriers for the H/F exchange processes.

Computational Studies

Reactant, Intermediate, and Product. The reaction path-ways that could account for the observed products of the reaction

(29) Harrison, R.; Heaney, H. *J. Chem. Soc. C* **1968**, 889.

between Cp′$_2$CeH, modeled by Cp$_2$LaH, **3**, and C$_6$F$_6$ and C$_6$F$_5$H were analyzed with DFT calculations with methodology that has been successful for the reaction of metallocene hydrides with H$_2$, CH$_4$, and CF$_4$ for the entire family of lanthanide elements.[30−34] These studies show no dependence of the nature of the lanthanide on the geometry of the metallocene except that due to the lanthanide contraction. They also show a minor dependence of the activation barrier of about 1 kcal mol^{-1} depending on the specific metal chosen. Therefore, the choice of using lanthanum, which lies to the immediate left of cerium and thus has a similar ionic radius, will not affect the calculated differences in energy to any significant extent. The numerical values calculated for La can be transferred to the case of Ce with an expected change of less than 1−2 kcal mol^{-1}. Modeling of Cp′ by C$_5$H$_5$ is a more severe approximation because of the large difference in steric size between these cyclopentadienyl ligands, especially when some significant geometrical reorganization can occur.[34−36] For this reason, two key structures were calculated with the QM/MM methodology using ONIOM (B3PW91:UFF). Calculated free energies, *G*, estimated at 298.15 K, are given in kcal mol^{-1} with respect to separated reactants Cp$_2$LaH and C$_6$F$_6$ or C$_6$F$_5$H. The entropy calculated in gas phase is exaggerated by around 50% with respect to what it is in the condensed phase at least for the particular case of a reaction in water.[37] Neglecting the translational part of the entropy as suggested by Sakaki could lead to an underestimation of the energy barriers for a bimolecular process.[38] Calculating the change in energy Δ*E* and in free energy Δ*G* for the model reactions gives similar conclusions and free energies are used throughout this paper.

Initially, the calculated geometries of reactant Cp$_2$LaH, **3**, and product Cp$_2$LaF, **4**, and an intermediate Cp$_2$LaC$_6$F$_5$, **5**, were optimized and compared to the solid-state structures of Cp′$_2$-CeH, Cp′$_2$CeF, and Cp′$_2$Ce−C$_6$F$_5$ (Figure 5). In **3**, the La−H bond length of 2.14 Å is reasonably close to the Ce−H distance of 1.9 Å, given the uncertainty of this datum. The Cp(centroid)−La distance of 2.56 Å is close to the experimental values of 2.55 and 2.51 Å. The smaller Cp(centroid)−La−Cp(centroid) angle of 134° relative to Cp′(centroid)−Ce−Cp′(centroid) angle of 155° is clearly due to the smaller size of C$_5$H$_5$ relative to 1,3,4-(Me$_3$C)$_3$C$_5$H$_2$. Similar trends were noted when comparing C$_5$H$_5$ and Me$_5$C$_5$ lanthanides derivatives.[34−36] In **4**, the La−F distance of 2.18 Å is slightly longer than the experimental Ce−F distance of 2.165(2) Å. The Cp(centroid)−La distance of 2.58 Å differs slightly from the experimental values in the Ce metallocene to ring distance of 2.57 and 2.53 Å, but the calculated Cp(centroid)−La−Cp(centroid) angle of 131° is again much smaller than the Cp′(centroid)−Ce−Cp′(centroid) angle of 149°. In the metallocene−pentafluorophenyl complex, **5**, the bidentate nature of the interaction between C$_6$F$_5$ and the metal is reproduced with La−C and La−F distances equal to 2.61
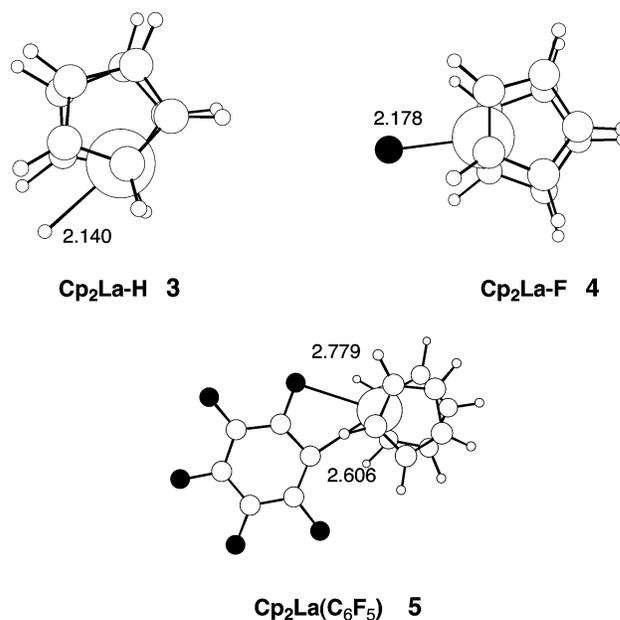
**Figure 5.** Optimized geometry (distance in Å, angles in degrees) of Cp$_2$-LaH, **3**, Cp$_2$LaF, **4**, and Cp$_2$La(C$_6$F$_5$), **5**; small white circle = H, medium white circle = C, large size white circle = La, medium black circle = F.

and 2.78 Å, respectively, compared to the experimental Ce−C and Ce−F distances of 2.621(4) and 2.682(2) Å. As before, the ring (centroid)−metal distances are comparable, 2.55 Å for Cp compared to 2.54 Å for Cp′, but the angle between the two rings is smaller with Cp (132°) than with Cp′ (147°). The Cp′-(centroid)−Ce−Cp′(centroid) angle gets smaller on going from H to F (155° and 149°, respectively); a smaller variation in the same direction is found in the calculated systems (134° for the hydride compared to 131° for the fluoride) because the Cp-(centroid)−La−Cp(centroid) angle is already very small.

Direct H/F Exchange. The first mechanism for H/F exchange tested by computational methods is to allow a fluorine atom in C$_6$F$_6$ to approach the metallocene hydride and then to allow a LaH···C(C$_6$F$_6$) and a La···F interaction to develop, that is, a σ bond metathesis transition state.[31,32,34,39,40] The transition state will look like **6** and involve a carbon at the β position of the kite-shaped transition state. This transition state looks attractive since the geometry around each atom is acceptable; in particular, the geometry of the carbon in the β position is pseudotetrahedral. Indeed, a molecular orbital calculation has suggested such a transition state[41] for which there is no experimental evidence.[40] Such a transition state looks like a planar cyclohexadienyl fragment with the positively charged metal center bonded to H and F. Despite considerable effort, no such transition state could be located on the potential energy surface for either C$_6$F$_6$ or C$_6$F$_5$H. The kite-shaped transition state geometry is clearly energetically unfavorable with carbon at the β position even when it is not hypervalent. One can speculate that the absence of such a transition state could be due to an electronic charge

(30) Maron, L.; Eisenstein, O. *J. Am. Chem. Soc.* **2001**, *123*, 1036.
(31) Maron, L.; Perrin, L.; Eisenstein, O. *J. Chem. Soc., Dalton Trans.* **2002**, 534.
(32) Perrin, L.; Maron, L.; Eisenstein, O. *Dalton Trans.* **2003**, 4313.
(33) Perrin L.; Maron L.; Eisenstein O. *Activation and Functionalization of C−H Bonds*; ACS Symposium Series 885; Goldman, A., Goldberg, K., Eds.; American Chemical Society: Washington, DC, 2004; pp 116−135.
(34) Scherer, E. C.; Cramer, C. J. *Organometallics* **2003**, *22*, 1682.
(35) Perrin, L.; Maron, L.; Eisenstein, O.; Schwartz, D. J.; Burns, C. J.; Andersen, R. A. *Organometallics* **2003**, *22*, 5447.
(36) Perrin, L.; Maron, L.; Eisenstein, O. *New J. Chem.* **2004**, *28*, 1255.
(37) Cooper J.; Ziegler, T. *Inorg. Chem.* **2002**, *41*, 6614.
(38) Sakaki, S.; Tatsunori, T.; Michinori, S.; Sugimoto, M. *J. Am. Chem. Soc.* **2004**, *126*, 3332.

(39) Steigerwald, M. L.; Goddard, W. A., III. *J. Am. Chem. Soc.* **1984**, *106*, 308. Rappé, A. K.; Upton, T. H. *J. Am. Chem. Soc.* **1992**, *114*, 7507. Rappé, A. K. *Organometallics* **1990**, *9*, 466. Ziegler, T.; Folga, E.; Berces, A. *J. Am. Chem. Soc.* **1993**, *115*, 636. Ziegler, T.; Folga, E. *J. Organomet. Chem.* **1994**, *478*, 57.
(40) Thompson, M. E.; Baxter, S. M.; Bulls, A. R.; Berger, B. J.; Nolan, M. C.; Santasierio, B. D.; Schaefer, W. D.; Bercaw, J. E. *J. Am. Chem. Soc.* **1987**, *109*, 203.
(41) Deelman, B.-J.; Teuben, J. H.; Macgregor, S. A.; Eisenstein, O. *New J. Chem.* **1995**, *19*, 691.
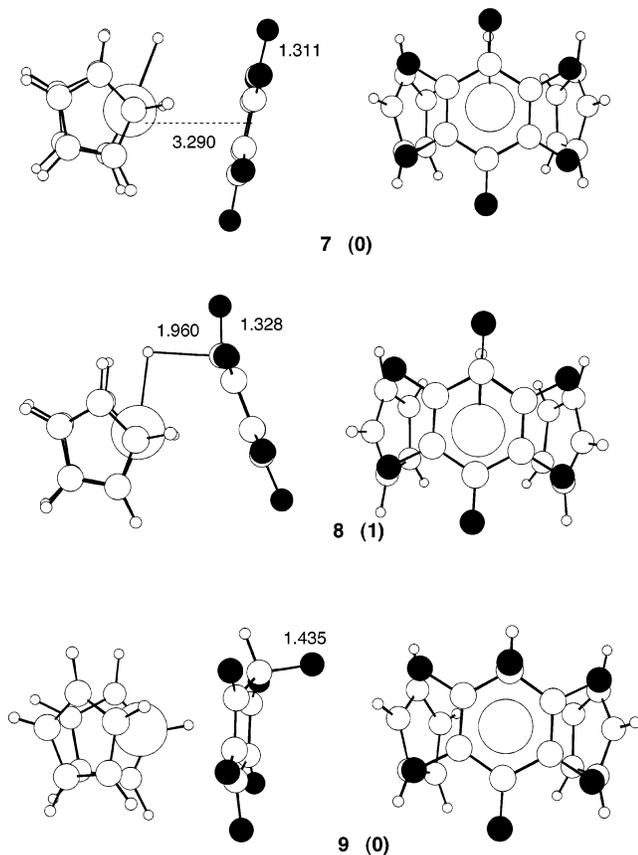
Figure 6. Two views of the optimized geometries (distances in Å) of the structures associated with H transfer to C_6F_6. The value in parentheses is the number of imaginary frequencies, 0 for a minimum, 1 for a transition state.

distribution poorly adapted for good stabilization. It is reasonable to assume that considerable density would be accumulated in the π system of the ring. However, the metal, which would be located nearby the $C(sp^3)-H$ and $C(sp^3)-F$ bonds, would be far from the part that should carry the negative charge and thus would have no stabilizing influence. This point of view is further supported by the location of a minimum for a structure with the metal bonded to the π system of the cyclohexadienyl ring as discussed in the following section.

6
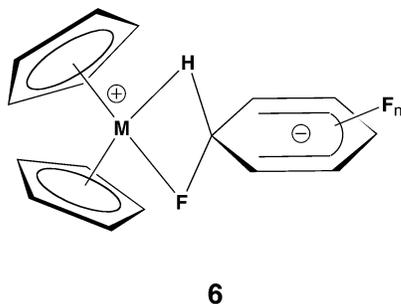
Hydride Addition to the Arene. An alternative mechanism is one in which the metallocene hydride adds to the six-membered ring since the electronegative fluorine makes the aromatic ring more of an electrophile. The result is adduct, **7**, in which the aromatic ring is perpendicular to the plane bisecting the Cp−La−Cp angle (Figure 6) and a C_6F_6(centroid)−La distance of 3.29 Å. The free energy of this π adduct **7** is 10.6 kcal mol⁻¹ above the separated reactants. From this adduct, a

transition state, **8**, 16.4 kcal mol⁻¹ above the separated reactants is reached. This transition state places the hydrogen only 1.96 Å from the ring carbon atom that is not yet significantly rehybridized, as the carbon atom is part of an essentially planar C_6F_6 ring. This transition state then connects to a cyclohexadienyl adduct, **9**, with the metal bonded almost equally to the five carbons of the pentadienyl fragment (2.9−3.0 Å) and 3.51 Å from the rehybridized carbon. The C−H bond is almost in the plane of the benzene ring while the C−F bond is almost perpendicular to it. The $C(sp^3)-F$ bond (1.435 Å) is longer than that calculated in CH_3F (1.382 Å), consistent with some delocalization of the π density into the $σ*_{CF}$ orbital. Structure **9** is calculated to be 16.1 kcal mol⁻¹ below the reactants. However, no path could be located that allows the Cp₂La fragment to abstract a fluorine. Migration of the metal fragment to a position between H and F is not possible since a transition state or a minimum of type **6** could not be located. Dissociation into separated metallocene ion and cyclohexadienyl anion is a most unlikely event, especially in a nonpolar solvent such as benzene. Therefore, the path **7 → 8 → 9** can only account for hydride transfer between the metal and the C_6F_6 ring. A reversible hydride transfer related to the calculated one has been observed in [(Ar*N=)(Ar*NH)Ta(H)(OSO₂CF₃)] (Ar*N = 2,6-(2,4,6 Me₃C₆H₂)₂C₆H₃N).[42] The bulkiness of the Cp′ ring also disfavors the transfer of the hydride since it requires the fluoroarene to be perpendicular to the plane bisecting the Cp−La−Cp angle in the adduct **7**, transition-state **8**, and cyclohexadienyl adduct **9**. To evaluate the destabilizing effect of the *tert*-butyl substituent, the adduct between C_6F_6 and Cp′₂LaH was calculated with the ONIOM method (Figure 7). The bulky Cp′ groups prevent the close approach of C_6F_6 to the metal as illustrated by the shortest distance La···C(C_6F_6) that increases from 3.48 to 5.15 Å upon replacing Cp by Cp′. In addition, whereas the C_6F_6 is approximately parallel to the La−H direction with Cp₂La−H, this is not the case with the Cp′ ligand. As a result, the attractive interaction between C_6F_6 and the metallocene hydride has decreased by 10.6 kcal mol⁻¹.[43] This pathway is disfavored by steric hindrance and involves a nonproductive hydride transfer and is therefore not considered further.

F/H Exchange via HF Formation. Alternative pathways therefore had to be developed and explored by calculations. Figure 7 shows that C_6F_6 can slide between the two cyclopentadienyl rings to point a fluorine atom toward the metal center even in the presence of the bulky *tert*-butyl groups. Thus, the free energy of the σ adduct of C_6F_6 and Cp₂La−H, **10**, is 8.2 kcal mol⁻¹ below the separated reactants. The CMe₃ groups destabilize the σ adduct by only 6.8 kcal mol⁻¹, that is, by less than for the π adduct.[43] In addition, the calculated La···F distance increases only moderately (from 2.746 to 3.084 Å) when replacing Cp by Cp′. The stability of the σ adduct illustrated by a free energy of dissociation of 8.2 kcal mol⁻¹ is significant and shows that a fluoroarene can bind to an electrophilic metal center by using a fluorine lone pair, a coordination mode observed for C_6F_6 with a cationic zirconocene.[44] The calculated La···F distance in **10** is also similar

(42) Gavenonis, J.; Tilley, T. D. *Organometallics* **2002**, *21*, 5549.
(43) This value is based on the differences in Δ*E* and not in Δ*G* because of the way frequencies are treated in the ONIOM method.
(44) Yang, X.; Stern, C. L.; Marks, T. J. *J. Am. Chem. Soc.* **1994**, *116*, 10015.

H...C(C6F6) = 3.172 (2.949)

La...C(C6F6) = 5.15 (3.48)

La...F = 3.084 (2.746)
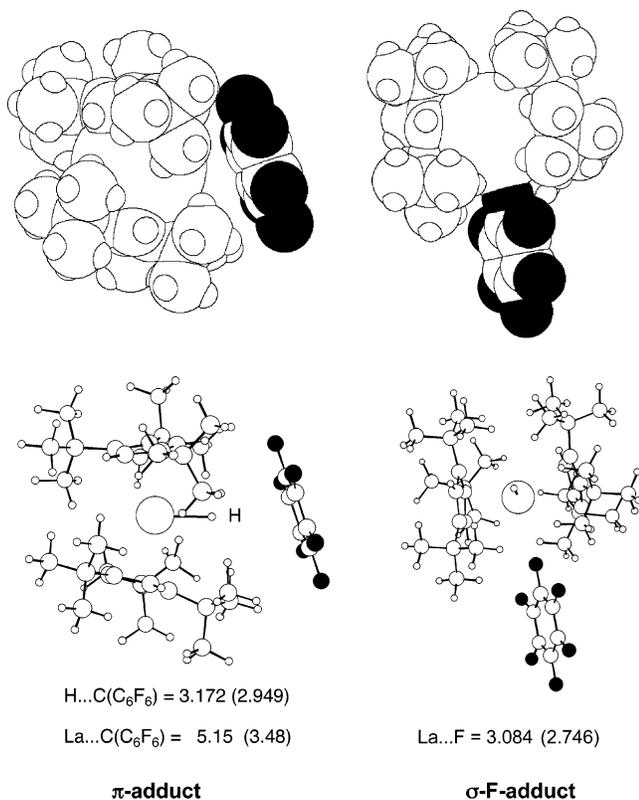
π-adduct

σ-F-adduct

Figure 7. Space-filling and ball-and-sticks representation of the optimized geometries of the π and σ adducts of C_6F_6 and Cp'_2LaH by the ONIOM (B3PW91:UFF) method. The distance given corresponds to the shortest one.
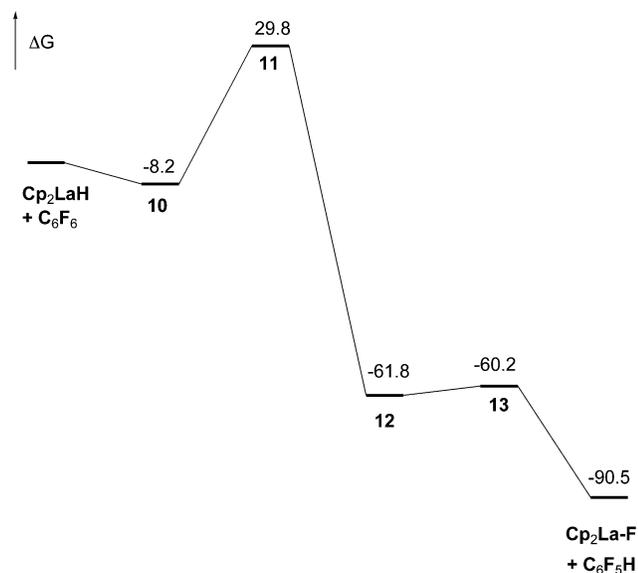
Figure 8. Free-energy profile ΔG (kcal mol^{-1} at 298.15 K) for the reaction of F/H exchange via HF formation.

to that calculated in $Cp_2La-C_6F_5$ illustrating the significant binding interaction.

Figure 8 shows the free-energy profile for the H/F exchange between Cp_2La-H and C_6F_6 starting with structure **10**, which is without direct participation of the arene π orbitals, and Figure 9 shows the structures of all extrema. In **10**, F(1) is only 1.84 Å from the hydride. A transition state, **11**, in which the C–F(1) bond is cleaved, is located 29.8 kcal mol^{-1} above separated reactants. From **11**, a rotation of the F···H atom pair in the plane
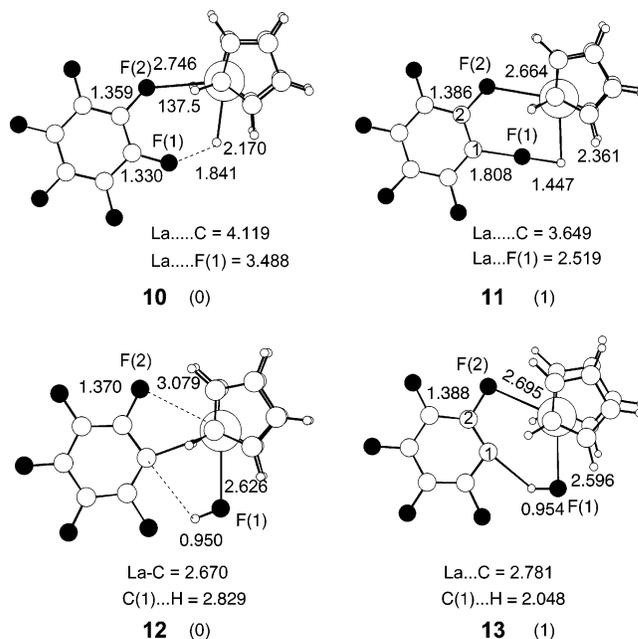
Figure 9. Optimized geometries of the extrema for the F/H exchange reaction via HF formation. The free energies are in kcal mol^{-1}. Large white circle = La, middle size white circle = C, small white circle = H, black circle = F. In parentheses, the number of imaginary frequencies, 0 for a minimum, 1 for a transition state.

bisecting the Cp–La–Cp angle forms $Cp_2La(C_6F_5)(FH)$, **12**, 61.8 kcal mol^{-1} below reactants. In **12**, the C_6F_5 group is bonded to La via C and F(2) as in $Cp_2LaC_6F_5$, **5**, but the La···F(2) distance is significantly longer because FH remains in the coordination sphere of the metal. This F–H adduct transforms, almost without activation energy via transition-state **13**, into Cp_2La-F and C_6F_5H with a total gain of free energy of 90.5 kcal mol^{-1} relative to reactants. This last step, which is formally a σ bond metathesis since it involves an interchange between the F–H and La–C bonds, is perhaps better viewed as a proton transfer from H–F to the negatively charged σ aryl group. During the proton transfer, the carbon of the fluoroarene moves away from the metal (2.67 and 2.78 Å in **12** and **13**, respectively), but this is compensated by a shortening of the La···F(2) bond (3.08 and 2.70 Å, respectively). This clearly emphasizes the key role of F(2) serving as a hook between the Cp_2La fragment and the arene so as to keep them in close proximity and lower the total free energy.

We have thus identified a pathway that transforms Cp_2La-H and C_6F_6 into Cp_2LaF and C_6F_5H, with one high but still accessible energy barrier associated with the C–F bond cleavage. At transition-state **11**, the carbon that loses its fluorine is not yet bonded to La (3.7 Å), while the hydride is (La–H = 2.4 Å), and C, F(1), and H are aligned. The alignment of C, F(1), and H allows the carbon to maintain some bonding interaction with F. The distance La···F(1) (2.52 Å) is rather short suggesting some bonding interaction. A remarkable aspect of this transition state is the reorganization of electronic charge that occurs on the way to **12**. In the reactant, **10**, the polarity of the σ bonds is C(1)$^{\delta+}$–F(1)$^{\delta-}$ and La$^{\delta+}$–H$^{\delta-}$ but in the product, **12**, the polarity is C(1)$^{\delta-}$–La$^{\delta+}$ and F(1)$^{\delta-}$–H$^{\delta+}$. Stated in another way, F(1) and La exchange partners, which demands that C(1) and H must also exchange their charges! In the initial adduct, **10**, the charge distribution is not very favorable because
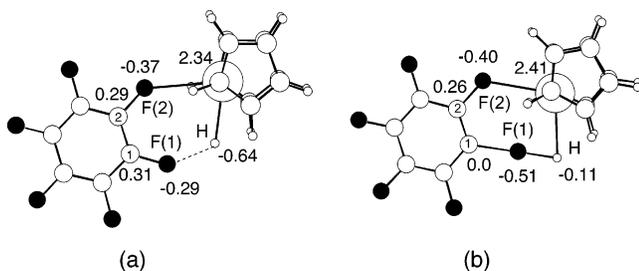
Figure 10. NBO charges on selected atoms in (a) the reactant **10** and in (b) the transition-state **11**.

Figure 11. Free-energy profile (kcal mol⁻¹ at 298.15 K) for the reaction Cp₂LaH + C₆F₅H → Cp₂LaF + C₆F₄ + H₂.
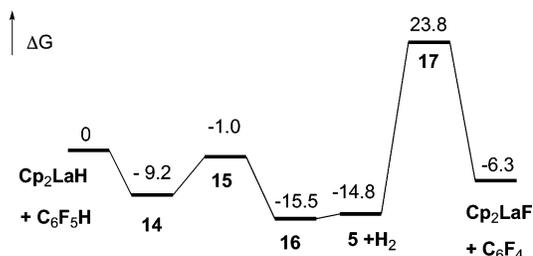
the negatively charged F(1) is relatively close to the hydride that also carries a negative charge and C(1) carries a positive charge. At this point, the change in NBO charges from the reactant **10** to the transition-state **11** shows the magnitude of the electron reshuffling (Figure 10). The relatively large positive charge at the metal remains almost constant from reactant (+2.34) to the transition state (+2.41) as do the charges on C(2) and F(2). Hence, all of the changes in the electron density occur between the hydride and the C(1)−F(1) bond that is cleaved. In the reactant, the hydride is strongly negatively charged (−0.64) while the charge on carbon is +0.31 and the fluorine is −0.29. The larger charge on the hydride relative to that on F(1) and even on F(2) illustrates the strong nucleophilic character of the hydride ligand. At the transition state, the hydride charge is only −0.11 while the charge on F(1) increases to −0.51 and the carbon charge decreases to nearly zero. The 0.5 electron density lost by the hydride is distributed to the carbon (0.3 e⁻ gained) and to the fluorine (0.2 e⁻ gained). This is consistent with a net transfer of density from the nucleophilic hydride to the σ^*_{C-F} weakening the C−F bond. This electron flow is necessary to form the final product as the hydride becomes protonic to bind to the fluoride. In this reorganization, the La⋯F(1) and La⋯C interactions develop. The electron redistribution is the reason for the high-energy barrier,[45] and any interaction that hinders the charge redistribution will raise the barrier.

The large thermodynamic driving force in the reaction is already apparent in the formation of **12** and is mostly associated with the formation of HF. However, formation of La−C₆F₅ bond also plays a role. The calculated ΔG of +22 kcal mol⁻¹ for the isodesmic reaction 6 illustrates this point.

$$Cp_2La-C_6F_5 + H-C_6H_5 \rightarrow Cp_2La-C_6H_5 + H-C_6F_5 \quad (6)$$
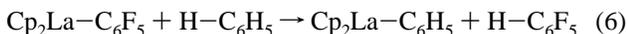
The H−C bond energy increases with F substitution on the arene but the energy of the M−C bond increases even more especially when there is a strong ionic character in the M−C bond,[46] which is the case for lanthanide species. There is thus an energy preference for the reactant side in eq 6.

Reaction of Cp₂LaH with C₆F₅H. In C₆F₆, all pathways necessarily involve a C−F activation step, which is not the case for C₆F₅H, where there is a choice between C−H and C−F activation. A path essentially identical to that calculated for C₆F₆ with an almost identical energy pattern (difference of about 1 kcal mol⁻¹ in the free-energy profiles and essentially identical geometries for the extrema) is found for the reaction of Cp₂-

(45) Shaik, S.; Shurki, A. *Angew. Chem., Int. Ed.* **1999**, *38*, 586.
(46) Clot, E.; Besora, M.; Maseras, F.; Eisenstein, O.; Oelckers, B.; Perutz, R. N. *Chem. Commun.* **2003**, 490.

LaH with C₆F₅H where the F/H exchange occurs at the position para to the existing C−H bond. This forms 1,2,4,5-tetrafluorobenzene and Cp₂La−F. However, we did not look at the energy profile for F/H exchange at the ortho or meta position with respect to the existing C−H bond, since there is no experimental evidence for these two isomers.

The free-energy profile is shown in Figure 11 and the geometry of the extrema is shown in Figure 12. The pathway involving C−H activation starts with the formation of an adduct **14**, in which an ortho F is coordinated to La and where the C−H bond points toward the hydride. This leads to the formation of a σ complex between Cp₂La−H and C₆F₅H, which has a geometry identical to **10**. From **14**, a transfer of hydrogen from carbon-forming Cp₂La(C₆F₅)(H₂) occurs in a moderately exergonic step (ΔG = −15.5 kcal mol⁻¹ below separated reactants), with a small activation barrier ($\Delta G^{\#}$ = 8.2 kcal mol⁻¹ above **14**) as it crosses the transition-state **15**. The transition state is clearly a proton transfer from C₆F₅−H to the hydride as shown by the alignment of the carbon, the transferring H, and the hydride. At the transition state, the carbon is not yet bonded to La (La⋯C = 3.04 Å). The transition-state **15** leads to a dihydrogen complex, Cp₂La(C₆F₅)(H₂), **16**, where H₂ hardly perturbes the geometry of free Cp₂La(C₆F₅). Dihydrogen loss from **16** occurs without change in free energy. From Cp₂La-(C₆F₅), **5**, C−F activation occurs with a significant activation barrier (23.8 kcal mol⁻¹ above separated reactants and 38.6 kcal mol⁻¹ above Cp₂La(C₆F₅)). The transition-state **17** produces C₆F₄ and Cp₂LaF. The overall transformation is exergonic compared to isolated Cp₂LaH and C₆F₅H even if trapping of C₆F₄ by C₆H₆ (C₆D₆ in the experiments) is not included in the modeling. However, the last elementary step (**5** → **17** → Cp₂-LaF + C₆F₄) is endergonic in the absence of trapping. When the trapping reaction is included, the free energy of the final species is −53.0 kcal mol⁻¹ compared to the path initiated by the C−F cleavage. The transition-state **17** for formation of C₆F₄ and Cp₂La−F shows an unusual orientation of the tetrafluorobenzyne ligand. Unlike all other ligands in this study, it does not lie in the plane bisecting the Cp−La−Cp angle but is significantly twisted out of it. This could be associated with a need for the very strongly electron deficient fluorinated benzyne to interact with the electron density of the Cp ring.

Interpretation of Experiments from Calculations. The experiments described show that the net H/F exchange reaction that results in formation of a Ce−F bond from a Ce−H bond is exothermic and rapid. The first resonances detected on mixing Cp′₂CeH and C₆F₆ in the ¹H NMR spectra are due to Cp′₂CeF, Cp′CeC₆F₅, and H₂. The dihydrogen is derived from the reaction of the metallocene hydride and C₆F₅H confirmed by independent experiment, which implies that the net rate constants for
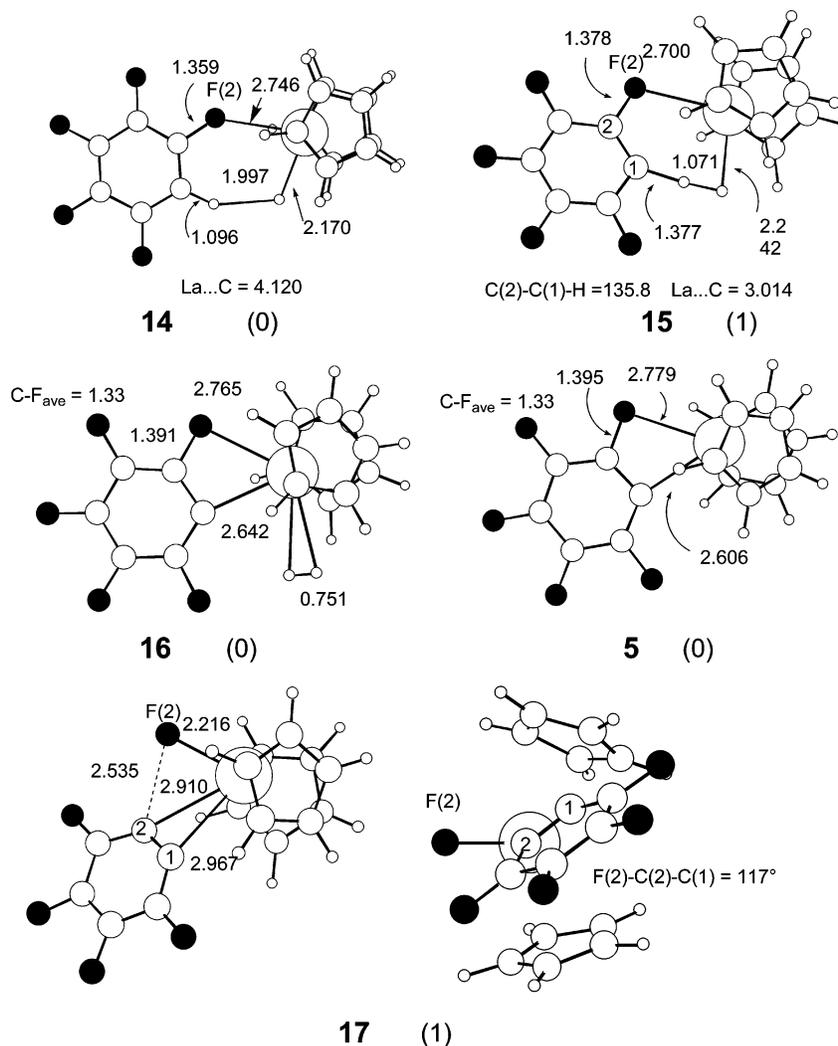
Figure 12. Optimized geometries of the extrema for the reaction of Cp$_2$LaH and C$_6$F$_5$H via successive C–H and C–F activation for formation of Cp$_2$LaF, C$_6$F$_4$, and H$_2$. The structures of reactant Cp$_2$La–H, C$_6$F$_6$, and products Cp$_2$La–F and C$_6$F$_4$ are not shown. The free energies are in kcal mol^{-1}. Large white circle = La, middle size white circle = C, small white circle = H, black circle = F. In parentheses, the number of imaginary frequencies, 0 for a minimum, 1 for a transition state.

formation of Cp′$_2$CeF from Cp′$_2$CeH and C$_6$F$_6$ or C$_6$F$_5$H are comparable since Cp′$_2$CeC$_6$F$_5$ and Cp′$_2$CeF are formed in comparable amounts even though the individual rate constants for intermolecular C–H and C–F activation are different. Calculations show comparable energy barriers for the rate-determining steps, which in both cases is cleavage of the C–F bond, although by different mechanisms. The calculated barriers of the reaction of Cp$_2$LaH and C$_6$F$_6$ or C$_6$F$_5$H indicate that the C–F activation barrier is about 4 times that for C–H activation. The calculated barrier for intramolecular C–F cleavage in going from Cp$_2$LaC$_6$F$_5$ to Cp$_2$LaF and C$_6$F$_4$ is comparable to that of the intermolecular C–F cleavage in the reaction of Cp$_2$LaH and C$_6$F$_6$. Once Cp′$_2$CeC$_6$F$_5$ is formed, two pathways are available for further reaction; in the presence of HF, a barrierless path to Cp′$_2$CeF and C$_6$F$_5$H, or in absence of HF, a high barrier path to Cp′$_2$CeF and tetrafluorobenzyne. The latter is then trapped by C$_6$H$_6$ or by Cp′ in a [2+4] cycloaddition that is Woodward–Hoffmann allowed. The slow rate for elimination of tetrafluorobenzyne is consistent with experiment, since Cp′$_2$CeC$_6$F$_5$ is an isolable compound and it decomposes to Cp′$_2$CeF and the Diels–Alder adduct, which is spectroscopically detected.

The calculated pathways provide a qualitative rational for the observed products of the reaction between Cp′$_2$CeH and C$_6$F$_6$ or C$_6$F$_5$H. The C$_6$F$_6$ can only react via C–F cleavage and the calculations show that C$_6$F$_5$H and the cerium fluoride complex, which is observed, are formed in a step that has a significant but presumably accessible barrier. As soon as C$_6$F$_5$H is formed, it can easily react via the C–H bond to form Cp′$_2$Ce–C$_6$F$_5$ complex and H$_2$, both of which are observed. The reverse reaction is not thermodynamically favored in agreement with experiment. The decomposition of the aryl complex to C$_6$F$_4$ and the cerium fluoride requires a high barrier, in agreement with the isolation of Cp′$_2$Ce(C$_6$F$_5$) and observation of its slow elimination of C$_6$F$_4$ that is trapped, which lowers the net free energy of the reaction. Figures 8 and 11 show that HF and H$_2$ are produced during the reaction but experimentally only H$_2$ is observed. This is no contradiction. The bonding between H$_2$ and the metal center is extremely weak (the calculations give no variation in ΔG upon loss of H$_2$), so H$_2$ is released as soon as it forms. The reaction of H$_2$ with the metallocene aryls is not expected to produce the metallocene hydride and the arene since this reaction is thermodynamically unfavorable. For

example, the transformation of Cp_2LaH and C_6F_5H into Cp_2-LaC_6F_5 and H_2 is exergonic by 14.8 kcal mol^{-1}. In 1,2,4,5-tetrafluorobenzene, the reaction is even more exergonic ($\Delta G = -21.9$ kcal mol^{-1}). Liberation of H_2 is thus expected and observed. In contrast, HF is more strongly bound and release of HF is energetically unfavorable. For example, the loss of HF from $Cp_2La(C_6F_5)(HF)$ is endergonic by 18 kcal mol^{-1}. Further, the addition of HF across the metal–carbon occurs with a low activation barrier so the HF formed is rapidly consumed to make Cp_2LaF and an arene with one less fluorine. Finally, the reaction of Cp_2LaH and HF leads first to $Cp_2LaH(FH)$ 1.5 kcal mol^{-1} below separated reactants, which transforms into Cp_2LaF and H_2 by going over a transition state that is 10.3 kcal mol^{-1} above the separated reactants. The final compounds Cp_2-LaF and H_2 are 62.8 kcal mol^{-1} below Cp_2LaH and HF. Therefore, any HF that is formed is consumed in production of the metal fluoride.

Epilogue

The calculations provide a reasonable framework to guide our understanding of the hills and valleys that the strongly exergonic H/F exchange reaction must traverse, without oxidative addition, reductive elimination sequences. The key points that emerge are (i) the activation barrier for C–H activation is lower than for C–F activation but the final product distribution is not determined by the relative barriers of these two processes. The calculated pathways show that the energy barriers for C–F cleavage from $Cp_2LaC_6F_5$ and for the reaction of Cp_2LaH and C_6F_6 are comparable. (ii) The F/H exchange occurs by initial coordination of the fluoroarene by the fluorine lone pairs in a σ type complex. The π orbitals of the arene are not directly involved in the F/H exchange. (iii) The formal bond metathesis that occurs between M–H and C–F to form M–C and F–H requires a strong electronic rearrangement at the transition state. During this process, the hydrogen atom in Ce–H that initially is hydridic becomes protonic, while the carbon that loses the F atom is initially positively charged and then neutral and then carbanionic. The electron flow that is associated with this electronic reorganization is different from that occurring in a typical σ bond metathesis and is the principal reason for the high barrier. (iv) Throughout the exchange reaction, the lone pair on the ortho-F is hooked to the electropositive metal center maintaining the translational entropy nearly constant. (v) The net result is that the thermodynamic favorable state is reached in a formal H/F exchange.

Experimental Details

General. All manipulations were performed under an inert atmosphere using standard Schenk and drybox techniques. All solvents were dried and distilled from sodium or sodium benzophenone ketyl. Fluoro- and hydrofluorobenzenes were dried and vacuum transferred from calcium hydride. Infrared spectra were recorded on a Perkin-Elmer 283 spectrometer as Nujol mulls between CsI plates. NMR spectra were recorded on Bruker AMX-300 or AMX-400 spectrometers at 19 °C in the solvent specified. ^{19}F NMR chemical shifts are referenced to $CFCl_3$ at 0 ppm. J-Young NMR tubes were used for all NMR tube experiments. Melting points were measured on a Thomas–Hoover melting point apparatus in sealed capillaries. Electron impact mass spectrometry and elemental analyses were performed by the microanalytical facility at the University of California, Berkeley. Samples for GC-MS were prepared from NMR reaction samples by adding a drop of D_2O or H_2O, agitating, and allowing the sample to stand closed for

10 min. The samples were then dried over magnesium sulfate, filtered, and diluted 10 fold with hexane. A 1-μL sample was injected into an HP6890 GC system with a J&W DB-XLB universal nonpolar column, attached to an HP5973 mass selective detector. The principle elution peaks consisted of free Cp'D and the fluorobenzyne to benzene cycloaddition products. The abbreviation Cp' is used for the 1,3,4-tri-*tert*-butylcyclopentadienyl ligand.

$Cp'_2CeOTf\cdot0.5$ Hexane. Cerium triflate[47] (15.0 g, 25.5 mmol) and Cp'_2Mg[48] (12.0 g, 24.5 mmol) were stirred at reflux in a mixture of pyridine (10 mL) and toluene for 24 h. The dark brown suspension was taken to dryness under reduced pressure. The residue was extracted with hexane (200 mL). The volume of the solution was reduced until precipitation occurred, warmed to dissolve the precipitate, and then cooled to −15 °C. The large brown crystals were recrystallized five times from hexane, until the crystals obtained were bright yellow in color. Yield, 11 g (14 mmol, 55%). MP 300−302 °C. ^1H NMR (C_7D_8): δ 4.16 (18H, $\nu_{1/2} = 75$ Hz), 1.25 (m, hexane), 0.88 (t, hexane, the integrated intensity of these two absorptions indicated about 0.5 hexane per metallocene), −5.36 (18H, $\nu_{1/2} = 60$ Hz), −13.66 (18H, $\nu_{1/2} = 60$ Hz). IR: 1340(s), 1240(m), 1220(m), 1210(m), 1190(m), 1180(m), 1170(w), 1020(s), 960(w), 830(m), 780(w), 690(w), 680(w), 640(s), 600(w), 550(w), 520(w), 450(w), 370(w) cm^{-1}. MS $(M)^+$ m/z (calcd, found) 755 (100, 100) 756 (41, 40) 757 (26, 25) 758 (8,8). Anal. Calcd for $C_{35}H_{58}CeF_3O_3S$ + 0.5 hexane: C, 57.1; H, 8.20. Found C, 57.2; H, 8.32.

$Cp'_2CeCH_2C_6H_5$. The triflate, $Cp'_2CeOTf\cdot0.5$ hexane (4.0 g, 5.0 mmol), was dissolved in 30 mL of diethyl ether and $C_6H_5CH_2MgCl$ (6.7 mL, 0.75 M in diethyl ether, 5.0 mmol) was added via syringe. The solution immediately changed from yellow to red and became cloudy within 5 min. After 5 min, the solvent was removed under reduced pressure and the red solid was extracted into 20 mL of pentane. The volume of the solution was reduced to 10 mL and cooled to −15 °C, giving red blocks. Yield, 2.1 g (3.0 mmol, 60%). MP 111−113 °C. ^1H NMR (C_6D_6): δ 13.25 (2H, $\nu_{1/2} = 245$ Hz), 4.29 (2H, $\nu_{1/2} = 20$ Hz), 2.47 (1H, $\nu_{1/2} = 14$ Hz), −0.53 (18H, $\nu_{1/2} = 190$ Hz), −1.80 (18H, $\nu_{1/2} = 195$ Hz), −13.19 (18H, $\nu_{1/2} = 45$ Hz), −32.62 (2H, $\nu_{1/2} = 280$ Hz). IR: 1590(s), 1490(s), 1370(s), 1360(s), 1240(s), 1220(m), 1210(w), 1170(w), 1160(w), 1030(w), 1000(m), 960(w), 930(m), 890-(w), 860(w), 820(m), 810(s), 790(m), 730(s), 720(w), 700(m), 690-(m), 680(m), 510(w), 440(w), 360(w) cm^{-1}. Anal. Calcd for $C_{41}H_{65}$-Ce: C, 70.5; H, 9.39. Found C, 70.3; H, 9.32. MS: no $(M)^+$ was observed but $(M-PhCH_3)^+$ was found m/z (calcd, found) 605 (100, 100) 606 (39, 43) 607 (17, 21) 608 (6, 6).

Cp'_2CeH. The benzyl, $Cp'_2CeCH_2C_6H_5$ (1.0 g, 1.4 mmol), was dissolved in 10 mL of pentane. The headspace in the Schlenk tube was evacuated and replaced with H_2 (1 atm). The red solution turned purple over 30 min. After 2 h, the volume of the solution was reduced until precipitation occurred and then warmed to dissolve the precipitate. Cooling to −15 °C yielded purple crystals. Yield, 0.76 g (1.2 mmol, 85%). MP 152−155 °C. ^1H NMR (C_6D_6): δ 31.86 (4H, $\nu_{1/2} = 220$ Hz), −3.44 (36H, $\nu_{1/2} = 45$ Hz), −12.45 (18H, $\nu_{1/2} = 45$ Hz). Neither the resonances nor the stretching frequencies of Ce−H were conclusively identified. IR: 2160(m), 1360(s), 1250(s), 1200(s), 1170(m), 1020(s), 1000(s), 960(m), 930(w), 920(w), 870(w), 840(w), 810(s), 800-(m), 790(w), 780(w), 680(s), 670(s), 600(m), 520(s), 480(w), 440(m), 360(s) cm^{-1}. MS: no $(M)^+$ was observed but $(M-2)^+$ was found m/z (calcd, found) 605 (100, 100) 606 (39, 43) 607 (17, 21) 608 (6, 6). Anal. Calcd for $C_{34}H_{59}Ce$: C, 67.2; H, 9.78. Found C, 67.5; H, 10.11.

Cp'_2CeF. The benzyl, $Cp'_2CeCH_2C_6H_5$ (1.0 g, 1.4 mmol), was dissolved in 10 mL of pentane and $BF_3\cdot OEt_2$ (0.09 mL, 0.032 g, 0.23 mmol) was added via syringe. The red solution immediately turned orange. The solution volume was reduced until precipitation occurred and then warmed to dissolve the precipitate. Cooling to −15 °C yielded

(47) Sofield, C. D.; Andersen, R. A. *J. Organomet. Chem.* **1995**, *501*, 271.
(48) Weber, F.; Sitzmann, H.; Schultz, M.; Sofield, C. D.; Andersen, R. A. *Organometallics* **2002**, *21*, 3139.

an orange powder. Yield, 0.44 g (0.70 mmol, 50%). MP 164−167 °C. ^{1}H NMR (C_6D_6): δ 20.00 (4H, $\nu_{1/2}$ = 70 Hz), −2.50 (36H, $\nu_{1/2}$ = 10 Hz), −6.81 (18H, $\nu_{1/2}$ = 10 Hz). IR: 2380(w), 2280(w), 2180(w), 1630-(w), 1590(w), 1350(s), 1270(w), 1260(m), 1240(s), 1200(s), 1170(s), 1110(m), 1090(m), 1020(m), 1000(s), 960(s), 930(w), 920(w), 870-(w), 810(s), 780(m), 700(m), 690(m), 680(s), 640(w) cm^{-1}. MS (M)$^+$ m/z = (calcd, found) 625 (100, 100), 626 (39, 40) 627 (20, 20) 628 (6, 5). Anal. Calcd for $C_{34}H_{58}CeF$: C, 65.2; H, 9.34. Found C, 65.3; H, 9.46.

Cp′((Me₃C)₂C₅H₂C(Me₂)CH₂)Ce. Cp′₂Ce(CH₂C₆H₅) (0.7 g, 1.0 mmol) was heated in pentane (10 mL) for 12 h. The red solution turned deep purple. The solvent was removed yielding a glassy solid. ^{1}H NMR (C_6D_{12}) δ 35.83 (1H, $\nu_{1/2}$ = 200 Hz), 33.71 (1H, $\nu_{1/2}$ = 158 Hz), 16.24 (3H, $\nu_{1/2}$ = 30 Hz), 5.97 (3H, $\nu_{1/2}$ = 50 Hz), −3.40 (9H, $\nu_{1/2}$ = 50 Hz), −5.63 (9H, $\nu_{1/2}$ = 45 Hz), −7.56 (9H, $\nu_{1/2}$ = 50 Hz), −10.10 (9H, $\nu_{1/2}$ = 10 Hz), −16.13 (9H, $\nu_{1/2}$ = 45 Hz), −29.25 (1H, $\nu_{1/2}$ = 110 Hz).

Cp′₂CeC₆H₅. Cp′₂Ce(CH₂C₆H₅) (1 g, 1.4 mmol) was heated at reflux in C_6H_6 (20 mL) for 3 days. The solution turned a deeper red and a small amount of yellow precipitate formed. The solvent was removed under reduced pressure and pentane (15 mL) was added. The solution was filtered, the volume was reduced to 10 mL, and the solution was cooled to −15 °C, giving a deep red powder. Yield, 123 mg (0.2 mmol, 14%). ^{1}H NMR (C_6D_6): δ 7.88 (1H, t), 6.12 (2H, d), −1.73 (36H, $\nu_{1/2}$ = 8 Hz), −10.48 (18H, $\nu_{1/2}$ = 11 Hz); the ortho proton resonance was not observed. Anal. Calcd for $C_{40}H_{63}Ce$: C, 70.2; H, 9.28. Found C, 70.1; H, 9.31.

{[C(CD₃)₃]₃C₅H₂}{[C(CD₃)₃]₂C₅H₂[C(CD₃)₂CD₂]}Ce. The benzyl, Cp′₂CeCH₂C₆H₅, was dissolved in C_6D_6 in an NMR tube. The sample was heated at 60 °C. After 6 days, the solution was taken to dryness. Fresh C_6D_6 was added, and the sample was heated at 60 °C for another 6 days. The solution was taken to dryness, and the deep red solid residue was dissolved in C_6D_{12}. The sample was heated for 1 day at 60 °C to generate the metallacycle. To determine the degree of deuteration of the Cp′-rings, a drop of degassed D_2O was added. GC MS analysis showed a mixture of Cp′D-d_{28}, Cp′D-d_{27}, and Cp′D-d_{26} in a 40:8:1 ratio, (M)$^+$ m/z (calcd, found) 260 (1, 1) 261 (18, 18) 262 (100, 100) 263 (19, 17) 264 (2, 2).

NMR Tube Reaction of {[C(CD₃)₃]₃C₅H₂}₂CeC₆F₅ in C_6D_{12}. A drop of C_6F_5H was added to the solution of the perdeuterated metallacyle. The deep purple solution rapidly turned orange. The ^{2}H and ^{19}F NMR spectrum showed resonances consistent with Cp′₂CeC₆F₅, and the ^{1}H spectrum showed only traces of undeuterated *tert*-butyl resonances. The solution was taken to dryness to remove excess C₆F₅H, and the orange residue was dissolved in C_6D_{12}. The sample was heated at 60 °C for 1 day and then hydrolyzed with a drop of degassed D_2O. The ^{19}F NMR spectrum indicated the formation of a new fluorine-containing species whose spectrum was not perturbed by the addition of D_2O. Analysis by GCMS showed one major component in addition to Cp′D-d_{28}, with (M)$^+$ m/z 410. This is believed to be the symmetric isomer of the [2+4] cycloaddition of tetrafluorobenzyne and Cp′D-d_{28}, **2**. Characterization of cycloaddition product: ^{19}F NMR (C_6D_{12}) δ −145.46 (2F, m), −158.78 (2F, m). GC MS analysis suggests a mixture of **2**-d_{28} and **2**-d_{27} in a 3:1 ratio, (M)$^+$ m/z (calcd, found) 409 (34, 32) 410 (100, 100) 411 (25, 33).

NMR Tube Reaction of Cp′((Me₃C)₂C₅H₂C(Me₂)CH₂)Ce and C_6H_6. Cp′₂Ce(CH₂C₆H₅) was dissolved in C_6D_{12} and the solution was heated at 60 °C for 12 h yielding Cp′((Me₃C)₂C₅H₂C(Me₂)CH₂)Ce. The solution was taken to dryness and the solid residue was dissolved in C_6H_6. The sample was heated at 60 °C for 3 days and then taken to dryness and the solid residue dissolved in C_6D_6. The ^{1}H NMR showed resonances characteristic of Cp′₂CeC₆H₅ and the integrated intensities indicated quantitative conversion.

NMR Tube Reaction of Cp′((Me₃C)₂C₅H₂C(Me₂)CH₂)Ce and H₂ in C_6D_{12}. Cp′₂Ce(CH₂C₆H₅) was dissolved in C_6D_{12} and the solution was heated at 60 °C for 12 h yielding Cp′((Me₃C)₂C₅H₂C(Me₂)CH₂)-

Ce. The tube was cooled in a liquid nitrogen 2-propanol bath, and the headspace was evacuated and replaced with CF₃H (1 atm). The tube was warmed to 19 °C and agitated. The ^{1}H NMR showed resonances whose integrated intensities indicated quantitative formation of Cp′₂-CeH.

Cp′₂Ce(C₆F₅). Cp′((Me₃C)₂C₅H₂C(Me₂)CH₂)Ce (0.6 g. 1 mmol) was dissolved in pentane (10 mL) and C₆F₅H (0.18 mL, 1 mmol) was added via syringe. The purple solution immediately turned orange. The solution volume was reduced to 5 mL and the solution was cooled to −10 °C, yielding orange crystals. The low yield was due to the high solubility of the compound. Yield: 0.15 g (0.19 mmol), 19%. ^{1}H NMR (C_6D_{12}) δ −1.77 (36H, $\nu_{1/2}$ = 190 Hz), −10.29 (18H, $\nu_{1/2}$ = 55 Hz), ^{19}F NMR (C_6D_{12}) δ −157.64 (1F, t, J = 18 Hz), −160.97 (2F, d, J = 18 Hz), −210.4 (2F, $\nu_{1/2}$ = 482 Hz). The solid material decomposed rapidly above 135 °C, which precludes analysis by EI-MS.

Cp′₂Ce(p-C₆F₄H). Cp′₂Ce(CH₂C₆H₅) was dissolved in C_6D_{12} and the solution was heated at 60 °C for 12 h yielding Cp′((Me₃C)₂C₅H₂C-(Me₂)CH₂)Ce. Three drops of 1,2,4,5-tetrafluorobenzene (an excess) were added to a clean NMR tube and the solution of Cp′((Me₃C)₂C₅H₂C-(Me₂)CH₂)Ce was slowly added with agitation. The solution turned from purple to orange. The ^{1}H and ^{19}F NMR spectra showed that Cp′₂-Ce(p-C₆F₄H) formed quantitatively. ^{1}H NMR (C_6D_{12}) δ 3.20 (1H, $\nu_{1/2}$ = 18 Hz), −1.84 (36H, $\nu_{1/2}$ = 130 Hz), −9.80 (18H, $\nu_{1/2}$ = 50 Hz), ^{19}F NMR(C_6D_{12}) −140.57 (2F, $\nu_{1/2}$ = 30 Hz), −241.5 (2F, $\nu_{1/2}$ = 410 Hz).

Cp′₂Ce(1,4-C₆F₄)CeCp′₂. Two NMR tubes containing equal amounts of concentrated solutions of Cp′₂Ce(CH₂C₆H₅) in C_6D_{12} were heated at 60 °C for 12 h yielding solutions of Cp′((Me₃C)₂C₅H₂C(Me₂)CH₂)-Ce. Three drops of 1,2,4,5-tetrafluorobenzene (an excess) were added to a clean NMR tube and one of the solutions of Cp′((Me₃C)₂C₅H₂C-(Me₂)CH₂)Ce was slowly added with agitation. The orange solution was taken to dryness to remove excess 1,2,4,5-tetrafluorobenzene, and the second solution of Cp′((Me₃C)₂C₅H₂C(Me₂)CH₂)Ce was added. ^{1}H NMR(C_6D_{12}) −1.98 (36H, $\nu_{1/2}$ = 200 Hz), −9.15 (18H, $\nu_{1/2}$ = 65 Hz), ^{19}F NMR (C_6D_{12}) −217.06 (2F, broad s). After 10 min, a yellow precipitate began to form. The solution was stored at room temperature for 1 day and then filtered. The insoluble yellow precipitate was suspended in C_6D_6 and heated at 60 °C for 1 day, yielding a clear yellow/orange solution. The ^{1}H NMR revealed resonances consistent with Cp′₂CeF.

Decomposition of Cp′₂Ce(1,4-C₆F₄)CeCp′₂ with H₂O. Cp′₂Ce(1,4-C₆F₄)CeCp′₂ was suspended in C_6D_{12} in an NMR tube, and a drop of degassed H_2O was added. The tube was agitated vigorously and then allowed to stand for 10 min. The solution was dried over $MgSO_4$ and filtered. The ^{1}H and ^{19}F NMR showed the presence of 1,2,4,5-tetrafluorobenzene.

Reaction of Cp′₂Mg and BrMgC₆F₅. Cp′₂Mg (0.35 g, 0.71 mmol) was dissolved in cyclohexane (5 mL) and BrMgC₆F₅ (1.6 mL, 0.22 M in diethyl ether, 0.35 mmol) was added.[49] The cloudy solution was stirred at reflux for 12 h, by which time the solution had turned bright pink. A drop of degassed water was added to an aliquot of the solution (1 mL). The complicated ^{19}F NMR spectrum contained six major signals, which appeared to correspond to two fluorine-containing compounds in a 1:1.5 ratio. GC MS analysis showed two primary components in addition to Cp′H, one with (M)$^+$ m/z 382 and one with (M-57)$^+$ m/z 325, in a 1:1.5 ratio. These are believed to be the two isomers of the [2+4] cycloaddition product of tetrafluorobenzyne and Cp′H, one symmetric and the other asymmetric, with the asymmetric isomer readily eliminating a *t*-Bu group. Characterization of symmetric isomer: ^{1}H NMR 4.19 (2H, s), 1.10 (36H, s), 0.45 (18H, s), ^{19}F NMR (C_6D_6) δ −145.32 (2F, D), −158.65 (2F, m). GC MS (M)$^+$ m/z (calcd, found) 382 (100, 100) 383 (26, 26) 384 (3, 3). Asymmetric isomer: ^{1}H NMR (C_6D_6) 3.99 (1H, s), 2.04 (1H, s), 0.92 (18H, s), 0.45 (18H, s), ^{19}F NMR (C_6D_6) δ −130.98 (1F, m), −147.20 (1F, m), −157.33

(49) Nield, E.; Stephens, R.; Tatlow, J. C. *J. Chem. Soc.* **1959**, 166.

(1F, m), −158.90 (1F, m). GC MS (M-57)⁺ *m/z* (calcd, found) 325 (100, 100) 326 (21,23) 327 (2, 2).

NMR Tube Reaction of Cp′₂CeC₆F₅ in C₆D₁₂. Cp′₂CeC₆F₅ was dissolved in C₆D₁₂ and the solution was heated at 60 °C for 12 h. The ¹H and ¹⁹F NMR spectra indicated the formation of Cp′₂CeF and a new fluorine-containing species whose spectrum was not perturbed by the addition of a drop of D₂O. GC MS analysis showed four primary components in addition to Cp′H, one with (M)⁺ *m/z* 382 and three with (M-57)⁺ *m/z* 325, in a 13:5:1:2 ratio. These are believed to be isomers of the [2+4] cycloaddition product of tetrafluorobenzyne and Cp′H, one symmetric and the others asymmetric, with the asymmetric isomers readily eliminating a *t*-Bu group. Characterization of the symmetric isomer: ¹H NMR (C₆D₁₂) 4.23 (2H, s), 1.22 (36H, s), 0.61 (18H, s),¹⁹F NMR (C₆D₁₂) δ −145.37 (2F, m), −158.72 (2F, m). GC MS (M)⁺ *m/z* (calcd, found) 382 (100, 100) 383 (26, 28) 384 (3, 3).

NMR Tube Reaction of Cp′₂CeC₆F₅ in C₆H₆. Cp′₂CeC₆F₅ was dissolved in C₆H₆ and the solution was heated at 60 °C for 12 h. The ¹H and ¹⁹F NMR spectra indicated the formation of Cp′₂CeF, the symmetric [4+2] cycloaddition product of Cp′H and tetrafluorobenzyne, and 5,6,7,8-tetrafluoro-1,4-dihydro-1,4-methanonaphthalene-*d₀*, the cycloaddition product of tetrafluorobenzyne to C₆H₆(Fruchier697). The latter two products were present in a 1:20 ratio. Characterization of 5,6,7,8-tetrafluoro-1,4-dihydro-1,4-methanonaphthalene-*d₀*: ¹H NMR (C₆D₆) δ 6.45 (4H, s) 4.77 (2H, s) ¹⁹F NMR δ −149.33 (2F, m), −161.91 (2F, m). GC MS (M)⁺ *m/z* (calcd, found) 226 (100, 100) 227 (13, 12).

NMR Tube Reaction of Cp′₂CeC₆F₅ in C₆D₆. Cp′₂CeC₆F₅ was dissolved in C₆D₆ and the solution was heated at 60 °C for 12 h. The ¹H and ¹⁹F NMR spectra indicated the formation of Cp′₂CeF, the symmetric [4+2] cycloaddition product of Cp′H and tetrafluorobenzyne, and 5,6,7,8-tetrafluoro-1,4-dihydro-1,4-methanonaphthalene-*d₆*, the cycloaddition product of tetrafluorobenzyne to C₆D₆.²⁵ The latter two products were present in a 1:10 ratio. Characterization of 5,6,7,8-tetrafluoro-1,4-dihydro-1,4-methanonaphthalene-*d₆*: ¹⁹F NMR (C₆D₆) δ −149.32 (2F, m), −161.96 (2F, m). GC MS (M)⁺ *m/z* (calcd, found) 232 (100, 100) 233 (14, 13).

NMR Tube Reaction of Cp′₂Ce(p-C₆F₄H) in C₆H₆. Cp′₂Ce-(CH₂C₆H₅) was dissolved in C₆D₁₂ and the solution was heated at 60 °C for 12 h yielding Cp′((Me₃C)₂C₅H₂C(Me₂)CH₂)Ce. Three drops of 1,2,4,5-tetrafluorobenzene were added to a clean NMR tube and the solution of Cp′((Me₃C)₂C₅H₂C(Me₂)CH₂)Ce was slowly added with agitation. The solution turned from purple to orange. The ¹H and ¹⁹F NMR spectra were consistent with quantitative formation of Cp′₂Ce-(p-C₆F₄H). The solution was taken to dryness to remove excess 1,2,4,5-tetrafluorobenzene and the solid residue was dissolved in C₆H₆. The sample was heated to 60 °C for 12 h. The solution was taken to dryness and dissolved in C₆D₆. The ¹H and ¹⁹F NMR spectra indicated the formation of Cp′₂CeF and 5,7,8-trifluoro-1,4,6-trihydro-1,4-methanonaphthalene-*d₀*, the cycloaddition product of 2,3,5-trifluorobenzyne to C₆H₆.²⁹ Characterization of 5,7,8-trifluoro-1,4,6-trihydro-1,4-methanonaphthalene-*d₀*: ¹H NMR δ 6.40 (4H, m) 6.08 (1H, m) 4.89 (2H, m) ¹⁹F NMR δ −126.74 (1F, m) −139.48 (1F, m) −152.68 (1F, m). GC-MS (M)⁺ *m/z* (calcd, found) 208 (100, 100) 209 (13,13).

NMR Tube Reaction of Cp′₂Ce(1,4-C₆F₄H) in C₆D₆. Cp′₂Ce-(CH₂C₆H₅) was dissolved in C₆D₁₂ and the solution was heated at 60 °C for 12 h yielding Cp′((Me₃C)₂C₅H₂C(Me₂)CH₂)Ce. Three drops of 1,2,4,5-tetrafluorobenzene were added to a clean NMR tube and the solution of Cp′((Me₃C)₂C₅H₂C(Me₂)CH₂)Ce was slowly added with agitation. The solution turned from purple to orange. The ¹H and ¹⁹F NMR spectra were consistent with quantitative formation of Cp′₂Ce-(1,4-C₆F₄H). The solution was taken to dryness to remove excess 1,2,4,5-tetrafluorobenzene and the solid residue was dissolved in C₆D₆. The sample was heated to 60 °C for 12 h. The ¹H and ¹⁹F NMR spectra indicated the formation of Cp′₂CeF and 5,7,8-trifluoro-1,4,6-trihydro-1,4-methanonaphthalene-*d₆*, the cycloaddition product of 2,3,5-trifluorobenzyne to C₆D₆.²⁹ Characterization of 5,7,8-trifluoro-1,4,6-trihydro-

1,4-methanonaphthalene-*d₆*: ¹H NMR(C₆D₆) δ 6.06 (1H, m) ¹⁹F NMR δ −126.74 (1F, m) −139.48 (1F, m) −152.68 (1F, m). GC-MS (M)⁺ *m/z* (calcd, found) 214 (100, 100) 215 (14,14).

NMR Tube Reaction of Cp′₂CeH and C₆F₆ in C₆D₆. Cp′₂CeH was dissolved in C₆D₆ and a drop of C₆F₆ was added. The solution immediately turned from purple to orange and gas bubbles were evolved. The ¹H and ¹⁹F NMR spectra showed resonances indicative of Cp′₂CeF and Cp′₂Ce(C₆F₅), C₆F₅H, and H₂. The cerium-containing species were present in a 3:2 ratio and accounted quantitatively for all of the Cp′₂CeH starting material. The sample was stored at room temperature for 7 days. The ¹H and ¹⁹F NMR spectra showed resonances indicative of Cp′₂CeF and 5,6,7,8-tetrafluoro-1,4-dihydro-1,4-metha-nonaphthalene-*d₆*, the [2+4] cycloaddition product of tetrafluorobenzyne and C₆D₆.

NMR Tube Reaction of Cp′₂CeH and C₆F₅H in C₆D₆. Cp′₂CeH was dissolved in C₆D₆ and a drop of C₆F₅H was added. The solution immediately turned from purple to orange and gas bubbles were evolved. The ¹H and ¹⁹F NMR spectra showed resonances indicative of Cp′₂CeF, Cp′₂Ce(C₆F₅), Cp′₂Ce(p-C₆F₄H), Cp′₂Ce(p-C₆F₄)CeCp′₂, and 1,2,4,5-tetrafluorobenzene. The cerium-containing species were present in a 3.5:2.5:1:4 ratio and accounted quantitatively for all of the Cp′₂CeH starting material. The sample was stored at room temperature for 7 days. The ¹H and ¹⁹F NMR spectra showed resonances indicative of Cp′₂CeF, 5,6,7,8-tetrafluoro-1,4-dihydro-1,4-methanon-aphthalene-*d₆*, and 5,7,8-trifluoro-1,4,6-trihydro-1,4-methanonaphtha-lene-*d₀*, the [2+4] cycloaddition products of tetrafluorobenzyne and 2,3,5-trifluorobenzyne to C₆D₆, respectively.

Computational Details

The Stuttgart−Dresden−Bonn relativistic large effective core potential (RECP)⁵⁰ has been used to represent the inner shells of La. The associated basis set augmented by an f polarization function (α = 1.000) has been used to represent the valence orbitals. F has also been represented by an RECP⁵¹ with the associated basis set augmented by two contracted d polarization Gaussian functions (α₁ = 3.3505-(0.357851), α₂ = 0.9924(0.795561)).⁵² C and H have been represented by an all-electron 6-31G(d, p) basis set.⁵³ The two-layer ONIOM calculations were carried out at the B3PW91:UFF level.⁵⁴ Calculations have been carried out at the DFT(B3PW91) level⁵⁵ with Gaussian 98.⁵⁶ The nature of the extrema (minimum or transition state) has been established with analytical frequency calculations and the intrinsic reaction coordinate (IRC) has been followed to confirm that transition states connect to reactants and products. The zero-point energy (ZPE) and entropic contribution have been estimated within the harmonic potential approximation. The Gibbs free energy, *G*, was calculated for *T* = 298.15 K. Following the tradition, we report geometrical parameters

(50) Dolg, M.; Stoll, H.; Savin, A.; Preuss, H. *Theor. Chim. Acta* **1989**, *75*, 173. Dolg, M.; Stoll, H.; Preuss, H. *Theor. Chim. Acta* **1993**, *85*, 441.
(51) Igel-Mann, H.; Stoll, H.; Preuss, H. *Mol. Phys.* **1988**, *65*, 1321.
(52) Maron, L.; Teichteil,C. *Chem. Phys.* **1998**, *237*, 105.
(53) Hariharan, P. C.; Pople, J. A. *Theor. Chim. Acta* **1973**, *28*, 213.
(54) Svensson, M.; Humbel, S.; Froese, R. D. J.; Matsubara, T.; Sieber, S.; Morokuma, K. *J. Phys. Chem.* **1996**, *100*, 19357. UFF stands for universal force field.
(55) Perdew, J. J. P.; Wang, Y. *Phys. Rev. B* **1992**, *82*, 284. Becke, A. D. *J. Chem. Phys.* **1993**, *98*, 5648. Burke, K.; Perdew, J. P.; Yang, W. In *Electronic Density Functional Theory: Recent Progress and New Directions*; Dobson, J. F., Vignale, G., Das, M. P., Eds.; Plenum: New York, 1998.
(56) Frisch, M. J.; Trucks, G. W.; Schlegel, H. B.; Scuseria, G. E.; Robb, M. A.; Cheeseman, J. R.; Zakrzewski, V. G.; Montgomery, J. A.; Stratmann, R. E.; Burant, J. C.; Dapprich, S.; Millam, J. M.; Daniels, A. D.; Kudin, K. N.; Strain, M. C.; Farkas, O.; Tomasi, J.; Barone, V.; Cossi, M.; Cammi, R.; Mennucci, B.; Pomelli, C.; Adamo, C.; Clifford, S.; Ochterski, J.; Petersson, G. A.; Ayala, P. Y.; Cui, Q.; Morokuma, K.; Malick, D. K.; Rabuck, A. D.; Raghavachari, K.; Foresman, J. B.; Cioslowski, J.; Ortiz, J. V.; Stefanov, B. B.; Liu, G.; Liashenko, A.; Piskorz, P.; Komaromi, I.; Gomperts, G.; Martin, R. L.; Fox, D. J.; Keith, T.; Al-Laham, M. A.; Peng, C. Y.; Nanayakkara, A.; Gonzalez, C.; Challacombe, M.; Gill, P. M. W.; Johnson, B. G.; Chen, W.; Wong, M. W.; Andres, J. L.; Head-Gordon, M.; Replogle, E. S.; Pople, J. A. *Gaussian 98,* Revision A.9; Gaussian, Inc.: Pittsburgh, PA, 1998.

with an accuracy of 10^{-3} Å and angles with an accuracy of 10^{-1} degrees although we often discuss the geometrical parameters with lesser accuracy because of the many approximations made in the modeling and in the level of calculation.

Supporting Information Available: Crystallographic data (also deposited with the Cambridge Crystallographic Data Centre; copies of the data (CCDC247161−247163) can be obtained free of charge via www.ccdc.cam.ac.uk/ data_request/ cif, by emailing data_request@ccdc.cam.ac.uk or by contacting The Cambridge Crystallographic Data Centre, 12, Union Road, Cambridge CB2 1EZ, UK; fax +44 1223 336033); labeling diagrams, tables giving atomic positions and anisotropic thermal parameters, bond distances, and angles, and least-squares planes for each structure, and list of energies and free energies for all calculated species. This material is available free of charge via the Internet at http://pubs.acs.org. Structure factor tables are available from the authors.

JA0451012